Variance reduction techniques for MCNP applied to PBMR

by

Marisa van der Walt De Kock

Mini-Dissertation submitted in partial fulfilment of the requirements for the degree Master of Science in Nuclear Engineering at the Potchefstroom Campus of the North-West University

Supervisor: Dr. Oscar Zamonsky

May 2009

ABSTRACT

The applicability of the Monte Carlo N-Particle code (MCNP) to evaluate reactor shielding applications is greatly improved through the use of variance reduction techniques. This study deals with the analysis of variance reduction methods, more specifically, variance reduction methods applied in MCNP such as weight windows, geometry splitting and source biasing consistent with weight windows.

Furthermore, different cases are presented to show how to improve the Figure of Merit (FOM) of an MCNP calculation when weight windows and source biasing consistent with weight windows are used. Various methodologies to generate weight windows are clearly defined in this dissertation.

All the above-mentioned concepts are used to analyse a system similar to the upper part of the Pebble Bed Modular Reactor's (PBMR) bottom reflector.

Declaration

I Marisa van der Walt De Kock, the undersigned, hereby declare that the work contained in this project is my own original work.

_____

Marisa van der Walt De Kock

Date: 17 April 2009

Centurion

Acknowledgments

I would like to show my appreciation to my supervisor Dr. Oscar Zamonsky and Dr. Onno Ubbink for their guidance, support and patience.

Coenie Stoker, Dr. Nic Coetzee, Eric Dorval, Ronald Sibiya, Sandy Van der Merwe and Gerhard du Preez thank you for your invaluable input and support.

Last but not least I would like to thank my husband Thys, my mother Marina and father Piet for their support and for believing in me.

Table of Contents

List of Figures

List of Tables

Abbreviations

Abbreviation or Acronym	Definition
FOM	*Figure of Merit*
MCNP	*Monte Carlo N-Particle Code*
PBMR	*Pebble Bed Modular Reactor*
TRISO	*Triple Coated Isotropic*
PDF	*Probability Density Function*
WW	*Weight Windows*
MeV	*Mega electron Volt*
MWe	*Mega Watt Electric*
MWt	*Mega Watt Thermal*
cm	*Centimetre*
sec	*Second*

Nomenclature

Variables or Constants	Definition
$C_s,\ C_u$	Constants
E, E'	*Energy*
H	*Operator*
H^+	*Adjoint Operator*
i	*Cell index*
I	*Source Intensity*
n	*Neutrons*
N	*Number of Histories*
P	*Phase Space*
P'	*Phase Space (Next Event)*
p	*Probability*
q	*Source density*
$\hat{q}$	*Source Probability density function*
q_{ex}	*External Source*
R	*Response*
R	*Radius*
R	*MCNP Relative Error*
$\mathbf{r_d}, \mathbf{r}$	*Position Vector*
T	*Computational Time*
t	*Time*
V_d	*Volume Element*
Vol_i	*Volume of a zone*
$W, w, \bar{w}', w'$	*Statistical Weight*
w_0	*Initial Weight*

$W_L,\ w_L$	*Lower Weight window bound*
W_U	*Upper Weight window bound*
$W_s,\ w_{survival}$	*Survival Weight*
$\overline{x}$	*Sample mean*
$\Omega', \hat{\Omega}'$	*Angle (Next Event)*
$\hat{\Omega}, \Omega$	*Angle*
ψ	*Angular Flux*
ψ^+	*Adjoint Angular Flux*
σ_S	*Macroscopic Scattering Cross-section*
σ	*Total Macroscopic Cross-section*
σ_f	*Macroscopic Fission Cross-section*
σ_a	*Macroscopic Absorption Cross-section*
σ_d	*Objective Function*
v	*Speed of a neutron*
∇	*Differential Operator*
σ_v	*MCNP Variance*
ϕ	*Scalar Flux*
ϕ^+	*Adjoint Scalar Flux*
γ, p	*Photons*
$\hat{n}$	*Normal vector*
Γ	*Surface*
δ	*Dirac delta Function*
imp	*Importance*
imp_R	*Importance in the right cell*
imp_L	*Importance in left cell*

1. INTRODUCTION

Lately there has been a worldwide renaissance in the nuclear industry due to the need for cleaner and cheaper energy. With this comes the opportunity for many new developments. In order to produce cheaper energy, new nuclear reactors are being designed and built. This in turn necessitates improved analysis tools and methods.

An important topic in reactor physics is the transport of neutrons and their interaction with matter. The governing equation describing neutron transport is the Boltzmann transport equation, which for a non-multiplying medium is expressed as (Lewis and Miller (1984)):

$$\frac{1}{v}\frac{\partial \psi}{\partial t}(\mathbf{r},\hat{\Omega},E,t)+\hat{\Omega}\bullet\nabla\psi(\mathbf{r},\hat{\Omega},E,t)+\sigma(\mathbf{r},E)\psi(\mathbf{r},\hat{\Omega},E,t)=q_{ex}(\mathbf{r},\hat{\Omega},E,t)+$$
$$\int dE'\int d\hat{\Omega}'\sigma_s(\mathbf{r},E'\rightarrow E,\hat{\Omega}'\bullet\hat{\Omega})\psi(\mathbf{r},\hat{\Omega}',E',t)$$

where ψ is the angular flux, $\hat{\Omega}$ is the direction of flight of the particle, $\mathbf{r}$ is the position vector, σ is the total macroscopic cross-section, σ_s is the macroscopic scattering cross-section, q_{ex} is the external source, E is the energy, t is the time and v is the speed of a neutron.

Shielding analysis forms a crucial part of reactor design. The public, operating personnel and reactor components must be protected against sources of radiation. Thermal and biological shields positioned in front of intense radiation sources are highly absorbent materials to photons and neutrons (Lamarsh and Baratta (2001)). Thermal shields prevent the embitterment of the reactor components, whereas biological shields protect people from neutrons and gammas. Typical shielding calculations performed in the industry are the transport of neutrons and gammas through large regions of shielding material.

The treatment of particle transport can be done by stochastic and deterministic methods.

This dissertation focuses on stochastic methods. The behaviour of radiation particles is a stochastic process based on a series of probabilistic events. These probabilistic events are characterized by random variables such as location, energy, direction of flight of the particle, mean free path[1] of the medium and type of interaction. (Radulescu (2003)).

The transport phenomena can be solved with the Monte Carlo method because radiation particles have a stochastic behaviour. The Monte Carlo code that will be used in this dissertation is the Monte Carlo N-Particle code (MCNP) (see Booth, *et al*. (2003)).

Monte Carlo codes can be used for the modelling of full geometrical detail of real-world systems. Another benefit of Monte Carlo codes is that they make use of continuous-energy cross-section data. For this reason, the application of the Monte Carlo method to solve shielding problems is steadily growing. The disadvantage associated with Monte Carlo codes is that they require long calculation times to obtain well converged results, especially when dealing with complex shielding systems. Figure 1 is a schematic representation of the advantages and disadvantages of Monte Carlo codes applied to the modelling of radiation transport through a shield.

[1] The mean free path is the average distance a particle will travel before having a collision.

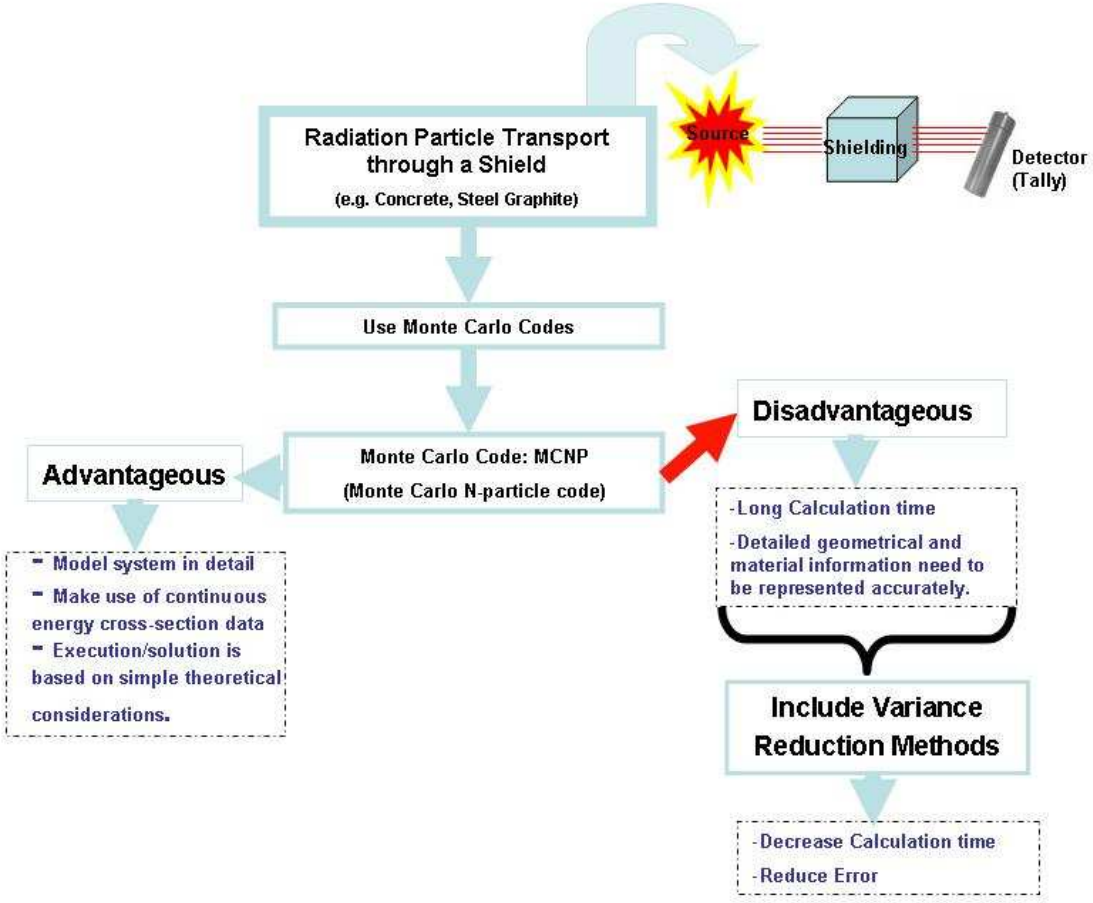

Figure 1: Advantages and Disadvantages of Monte Carlo Codes

In order to shorten the calculation time and to decrease the error of the results obtained with Monte Carlo methods, i.e. to improve the efficiency of a Monte Carlo calculation, variance reduction techniques must be used.

The usage of variance reduction methods in MCNP is not straightforward. There is a danger that these methods may be used as a black box leading to results not being analysed correctly or results being misinterpreted. This dissertation presents a methodology on how to use some of these variance reduction methods. The methods used and discussed are (Booth, et al., (2003)):

- Geometry truncation, which entails the truncation of the geometry so that unnecessary time is not spent following particles not important for the MCNP tally (truncation class).

- Weight windows forms part of the population control class and is a space-energy-dependent splitting and Russian roulette technique. This is discussed in more detail in Chapter 2.
- Ring detectors, which fall within the partially deterministic method class and work on the basis of avoiding the random walk[2] process by using deterministic-like techniques instead. These techniques include next event estimators or controlling the random number sequence.
- Source biasing, which is part of the modified sampling class. This method changes the statistical sampling of a problem. With this method it is possible to sample from an arbitrary distribution, instead of sampling from physical probability. This will be discussed in more detail in Chapter 3.

A general discussion on concepts like the adjoint flux, statistical weight and importance of a region is presented in this dissertation. The methodology followed in this study is to investigate these concepts and variance reduction techniques.

Different case studies are defined to outline these separate effects. For each case study, the weight windows for the different systems are generated with MCNP. Various approaches for determining the weight windows are discussed.

One of the main purposes of this dissertation is to investigate whether the statistic indicators of an MCNP calculation improve when variance reduction methods such as weight windows and source biasing consistent with weight windows are applied. The weight windows generated are used not only to improve the sampling in the system but also to bias the source. The source is biased through a biased source probability density function that guarantees that the weights of most of the source particles are within the weight window bounds. The influence of both weight windows and source biasing on the statistics of the results are analysed in the cases solved. This process will be discussed in detail in Chapter 3.

A graphite cylinder similar to the upper part of the bottom reflector of the PBMR is used as a typical test to demonstrate the abovementioned concepts. The Pebble Bed

[2] A random walk is a selection of events for a particle history.

Modular Reactor is a 400 MWt nuclear reactor. This reactor is designed to use Triple Coated Isotropic (TRISO) fuel particles embedded in six centimetre diameter graphite spheres with a projected electricity output of 165 MWe. The term 'modular' is from the design intent that identical modules can be placed in a block of four to eight reactors to make up a large power station (Koster (2008)). The PBMR has centre, side, bottom and top reflectors. The bottom reflector that is considered in this study is discussed in Chapter 5.

1.1 Research Objectives

The objective of this study is to analyse some variance reduction techniques for probabilistic methods applied to transport calculations. Different approaches have been investigated to optimize and analyse the variance reduction methods. A simplified PBMR system is used to apply some of the conclusions obtained.

The objectives of this dissertation are:

- To show examples on several procedures to generate weight windows for different systems;
- To show how variance reduction methods improve the efficiency of an MCNP calculation;
- To show how to bias the source by using weight windows;
- To analyse coupled neutron-photon problems with photon tallies and to show how weight windows generated for a coupled neutron-photon problem can be used for an photon-only problem; and
- To apply all the above to a system similar to the top part of the PBMR bottom reflector.

1.2 Layout of Dissertation

This dissertation is presented in seven chapters. Chapter 2 provides a review of the available literature relevant to this study. Literature covered is the Monte Carlo method, the MCNP (Monte Carlo N-particle) code and variance reduction methods.

Mathematical derivations are presented in Chapter 3 to explain the concepts of adjoint flux, statistical weight, importance and source biasing.

In Chapter 4 different case studies are defined to outline separate effects. For each of these case studies a methodology is given on how to generate weight windows for the system. It is also shown how these weight windows are used to determine the source biasing parameters. Some comparisons between cases with no weight windows, with only weight windows and source biasing consistent with weight windows, are performed to determine the extent of the improvement of the MCNP statistics. It is also shown how weight windows generated for a coupled neutron-photon problem can be used for a photon-only problem.

Chapter 5 presents the case study which is a graphite system similar to the top part of the bottom reflector of the PBMR. All the concepts and methodologies defined in this dissertation are applied to this case study.

The conclusions of this work are given in Chapter 6 and the bibliography is given in Chapter 7.

2. Literature Survey

This chapter gives a general review of the literature available on the Monte Carlo method, Monte Carlo applied to particle transport, the MCNP code and some variance reduction methods. Variance reduction methods form an important part of this dissertation therefore the basic theory of geometry splitting and weight windows are included in this chapter.

2.1 Monte Carlo Method

Monte Carlo methods are often used when simulating physical and mathematical systems. They are a class of computational algorithms that rely on repeated random sampling to compute their results. This section discusses some background on the Monte Carlo method.

2.1.1 Monte Carlo in General

Scientific computing in general and, more specifically, Monte Carlo methods date back as far as the 1940s. Von Neumann, Fermi, Ulam and Metropolis played major roles in research to define the basis of Monte Carlo methods (Brown (2000)).

It was shown that Monte Carlo methods are highly accurate but expensive (in terms of calculation time). Monte Carlo codes work effectively on all types of computer architectures such as vector, parallel, supercomputers, workstations, PC's, Linux clusters.

The Monte Carlo method is an efficient tool to be used in processes that have random behaviours, such as:

- High-energy physics
- Particle transport
- Financial analysis
- Process engineering

2.1.2 Monte Carlo and Particle Transport

Monte Carlo methods make use of a pseudo random number generator to simulate particle histories. Random numbers are generated with each particle history and used to sample probability distributions, e.g. scattering angles, track lengths distances between collisions.

The Monte Carlo sampling process, as discussed in detail in Ozgener (2006), is summarized below.

Consider a fixed source in a non-multiplying medium with only capture and elastic scattering. Each history begins by sampling the source distribution in order to determine the particle's initial energy, position and direction. After stochastically determining the distance that the particle will travel before colliding, the material region and point of collision are determined. By sampling cross-section data, it is determined with which nuclide the particle collided and whether the collision is a capture or a scattering reaction. If it is a scattering reaction, the distribution of scattering angles must be sampled to give a new direction. In the case of elastic scattering, a new energy is determined by the conservation of energy and momentum. Once the energy, position and direction have been determined after a collision, the above procedure is repeated for successive collisions until the particle is absorbed or escapes from a system.

Figure 2 shows the lifecycle of the neutron based on the analog Monte Carlo calculation model. The analog model makes use of natural probabilities that events such as collisions, fission and capture may occur. Thus, the analog model is directly analogous to the way in which the transport occurs naturally.

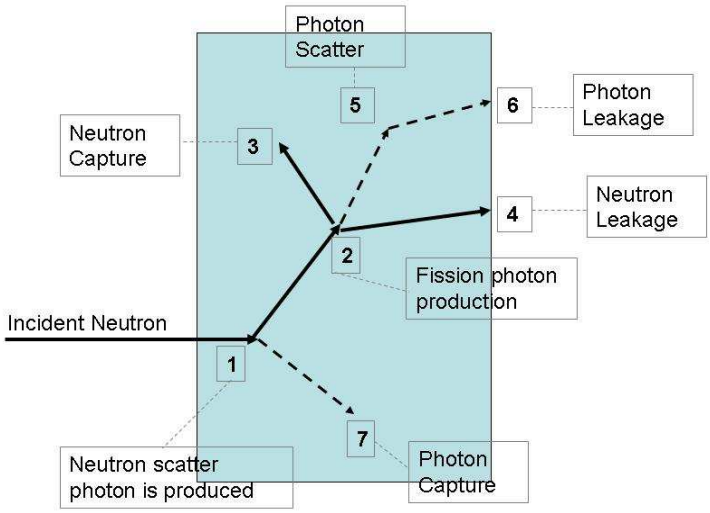

Figure 2: Lifecycle of a Neutron (see Booth, *et al.*, (2003))

The application of the analog model to shielding problems can be very inefficient. This is because most of the calculation time is spent on particle histories that do not contribute significantly to the result. In this case Monte Carlo fails because only a few particles are detected, leading to unacceptable uncertainties in the results (see Booth, *et al.*, (2003))., There are variance reduction techniques that can be used to improve the efficiency of the Monte Carlo calculations. These are described below.

2.2 MCNP Code

The Monte Carlo N-Particle (MCNP) code and some of its features are discussed in this section (see Booth, et al. (2003)). MCNP version 5 is the main shielding and criticality analysis tool used by the radiation transport group at PBMR and will be used in this study.

MCNP is useful for complex geometry problems that at this time cannot be modelled efficiently with computer codes that, use deterministic methods, for example. The code has the capability of dealing with continuous energies, generalized geometries and time-dependent problems. The code deals with the transport of neutrons, photons, electrons, combined neutrons and photons where the photons are produced by neutron interactions, combined neutrons, photons and electrons, or combined photons and electrons.

MCNP user input is file-based. The input file, created with any generic editor such as Multi-Edit™, contains the geometrical description of the model system, the description of materials for the system and a selection of cross-sections. The location and the characteristics of the neutron, photon or electron source, the type of answers or tallies and variance reduction methods that are needed to improve the efficiency of the calculation, are also specified in the input file.

MCNP has the functionality of providing the user with information such as the population of particles in a cell, the weight balance of each cell and much more not discussed here. The types of tallies used in this dissertation are a surface current tally, a track length estimate of cell flux tally and ring detectors.

2.2.1 MCNP Statistics

This section explains some of the statistical tests in the tally fluctuation chart. The tally fluctuation chart is automatically printed in the MCNP output file to show some statistical indicators that give an idea of the convergence of a solution. In general, a solution has to pass all the built-in MCNP statistical tests in order to be considered as converged. All these tests are explained in detail in the MCNP manual (Booth, *et al*. (2003)). A brief discussion on only the tally mean, relative error, and figure of merit follows because the main interest is only to show the improvement of these statistic indicators due to the variance reduction methods applied in this study.

2.2.1.1 The Tally Mean

The tally mean is given as:

$$\overline{x} = \frac{1}{N}\sum_{i=1}^{N} x_i \tag{2.2.1}$$

where x_i is the value of x selected form $f(x)$ for the i^{th} history and N is the number of histories. The function $f(x)$ is the probability density function for selecting a random walk that scores x to the tally being estimated. The tally mean $\overline{x}$ is the average value of the scores x_i for all the histories calculated in the problem.

When considering the tally fluctuation chart in the MCNP output file it should be verified that for the last part of the MCNP calculation there are no upward or downward trends in the mean.

2.2.1.2 The Relative Error

The relative error in MCNP is given by:

$$R = \left(\frac{\sigma_v}{\sqrt{N}} \right) / \bar{x}, \tag{2.2.2}$$

where σ_v^2 is the sampled history variance. It can be seen that $R \propto \frac{1}{\sqrt{N}}$ and the calculation time T is proportional to N. In order to reduce R the value of σ_v has to be decreased or N has to be increased. It is not always efficient to increase N, since in order to reduce the relative error by a factor of 10, N needs to be increased by a factor of 100. Decreasing σ_v can be done by using variance reduction techniques.

The relative error indicates the precision of the tally mean. Table 1 (see Booth, *et al.* (2003)) must be used in the assessment of the relative error of the MCNP tally. From the table given below, it is also clear that when using ring detectors, one should make sure that the relative error is less or equal to 0.05 in order to have meaningful and reliable results.

Table 1: Judging an MCNP Tally (from the MCNP Manual (Booth, *et al.* (2003))

Range of Relative Error	Quality of MCNP Tally
>0.5	Meaningless (not reliable confidence intervals)
0.2 to 0.5	Factor of a few (not reliable confidence intervals)
<0.1	Reliable excluding point and ring detectors
<0.05	Reliable for all tallies including point and ring detectors

The relative error is proportional to the inverse of the square root of the number of histories; therefore the relative error should decrease monotonically during an MCNP calculation.

2.2.1.3 The Figure of Merit

The Figure of Merit (FOM) is an important MCNP measurement that indicates the efficiency of calculations. The figure of merit is defined as (Booth (1985)):

$$FOM = \frac{1}{R^2 T} \tag{2.2.1}$$

where T is the calculation time. The behaviour of the figure of merit in the tally fluctuation chart should be roughly constant and the value for the FOM should be large. The larger the FOM the more efficient a Monte Carlo calculation becomes because less time is required to reach a given R. The FOM can be improved by applying variance reduction methods. In light of this dissertation, it will be shown how the FOM is increased when weight windows and source biasing consistent with weight windows are applied.

2.3 Variance Reduction Techniques

This section discusses the basic theory of some variance reduction methods used in this dissertation.

Variance reduction techniques are used in the MCNP code to increase the speed of a calculation and to enhance the precision of the results. Generally these techniques will lead to a decrease in the variance of the statistics of the results and/or a decrease in the calculation time, causing an increase in the figure of merit.

Monte Carlo variance reduction techniques can be divided into four classes (Culbertson and Hendricks (1999)), namely:

- The truncation method (geometry truncation, time and energy cut-off);
- The population control method (Russian roulette, geometry splitting and weight windows);
- The modified sampling method (source biasing); and

- The partially deterministic method (point detectors, DXTRAN).

The various variance reduction techniques in MCNP are all explained in detail in the MCNP manual (Booth, *et al*. (2003)). The methods used in this study, such as weight windows, source biasing and geometry splitting, are explained in the following sections.

2.3.1 Implicit capture

An interesting example of an analog event is the treatment of an analog capture in a Monte Carlo calculation. If w_0 is the initial weight of the particle, the weight w' that the particle will have after a collision can be described with the following scheme:

$$w_0 \rightarrow \begin{cases} p = \dfrac{\sigma_s}{\sigma} & w' = w_0 \\ p^* = 1 - p & w' = 0 \end{cases} \Rightarrow \bar{w}' = pw_0 + p^* \times 0 = \frac{\sigma_s}{\sigma} w_0$$

where p is the probability of the particle being scattered after a collision, σ_s is the scattering macroscopic cross-section and σ is the total macroscopic cross-section. In the previous equation $\bar{w}'$ is the expected outcome of the weight.

It has been shown that the efficiency of a Monte Carlo calculation is improved when using implicit capture instead of analog capture. This is a variance reduction technique where a particle is never killed if absorbed; it is only killed when its weight is below a user-specified survival weight. For the implicit capture the particle always survives a collision with weight:

$$w' = \frac{\sigma_s}{\sigma} w_0$$

Note that the expected weight after each collision is the same as in the case of an analog capture, meaning that the implicit capture is an unbiased variance reduction technique.

A technique called weight cut-off is used to avoid continuing sampling particles with very low weight. This technique is described below in this chapter.

2.3.2 Geometry Splitting with Russian Roulette

In order to apply this technique, a distribution of importances must be provided for the cells involved in the geometry modelled for an MCNP calculation. When particles move to a more important region, the number of particles is increased to provide better sampling and the weight of the particle is halved. If the particles move to a less important region, they are killed in an unbiased way to prevent wasting time on them. Splitting increases the calculation time and decreases the history variance, whereas Russian roulette does the complete opposite. Figure 3 illustrates how geometry splitting is applied when a particle is transported from one cell with a lower importance to another cell with higher importance.

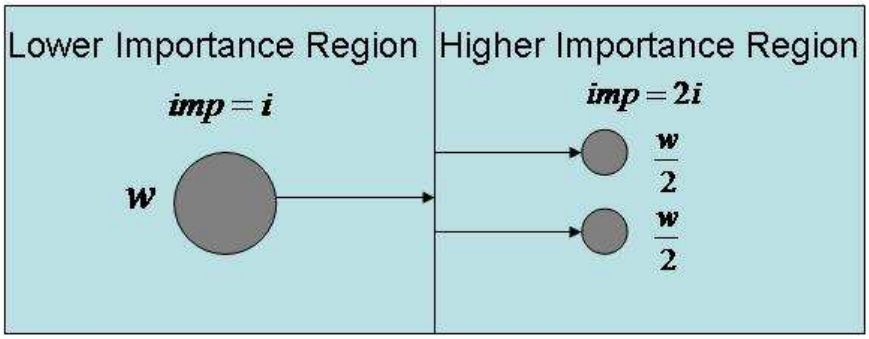

Figure 3: The Splitting Process

It can be seen from Figure 3 that the total weight of the particles is preserved in the splitting process.

Figure 4 presents a particle with weight w that moves from a region with higher importance (imp_R) to a region with lower importance (imp_L) and shows the Russian roulette process.

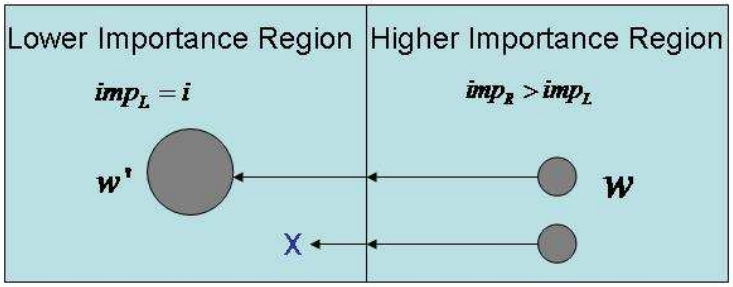

Figure 4: The Russian Roulette Process

When the Russian roulette process is applied to a particle, the particle will survive with weight $w' = w\frac{imp_R}{imp_L}$ with a probability $p = \frac{imp_L}{imp_R}$ and the particle is killed with probability $1-p$. This method is also an unbiased method since the expected outcome of the weight is equal to $p\,w' = w$. Therefore, the conclusion can be made that both splitting and Russian roulette are unbiased processes.

2.3.3 Weight Windows

In order to use weight windows in MCNP it is required that the user supplies an upper weight bound and a lower weight bound, W_U and W_L shown in Figure 5 respectively. These weight bounds therefore define a window with acceptable weights.

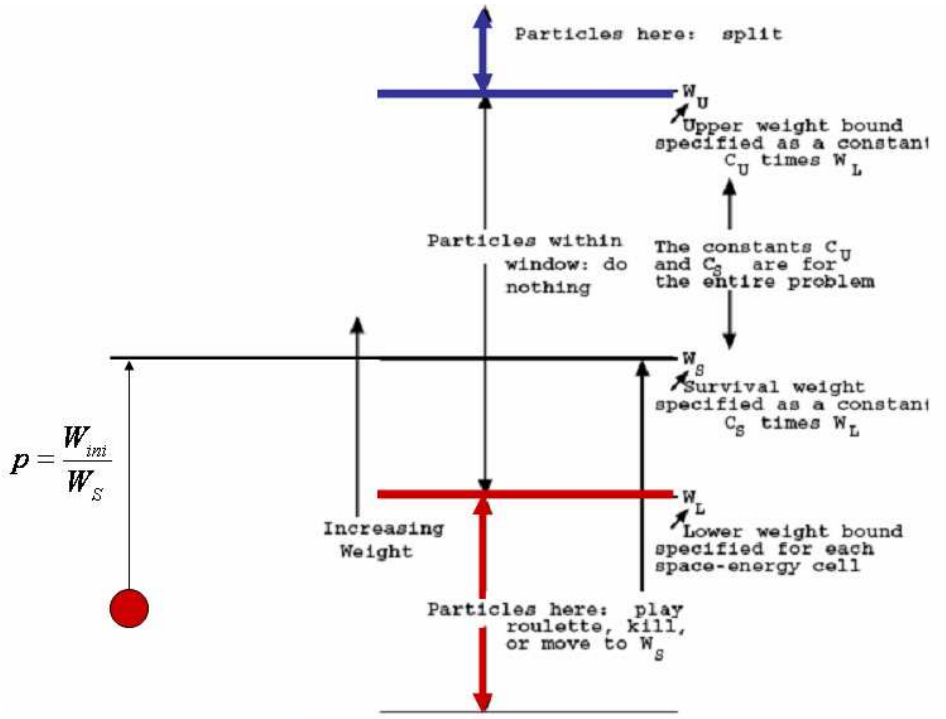

Figure 5: Description of the Weight Windows Technique (Booth, *et al.* (2003))

If a particle has a weight equal to W_{ini} (the red particle in Figure 5), which is lower than W_L, the particle will undergo Russian roulette with a survival weight equal to W_S which is also provided by the user. Note that W_S has to be between the window defined by W_U and W_L. If W_{ini} is greater than W_U, the particle is split into a predefined number of particles until all the particles are within the window. If W_{ini} is within the window the particle continues with the same weight. Note that the weight windows technique is unbiased since all the processes (splitting and Russian roulette) used to manage the weight of the incoming particle are unbiased.

One problem that may arise when using weight windows is that over-splitting might occur when a particle enters a region or it is born in a region with much higher weight than the upper limit of the weight windows in that region. This can usually be solved by modifying some of the weight window parameters, e.g. the normalization factor that MCNP applies to a weight windows distribution or the size of the weight windows mesh.

There is an automatic weight windows generator in MCNP. This generator statistically estimates the weight windows distribution in a system by using the cell's importance, which is estimated as:

$$\text{Importance} = \frac{\text{Total score because of particles (and their progeny) entering the cell}}{\text{Total weight entering the cell}} \qquad (2.2.2)$$

The lower weight of the weight windows is then defined as the inverse of the importance calculated with Equation (2.2.2).
Since this is a statistical estimator, the system must be well sampled to obtain an accurate weight windows distribution throughout the system.

2.3.3.1 Comparison of Weight Windows and Geometry Splitting

Both the weight window technique and geometry splitting make use of Russian roulette. Therefore, the question, about what the difference between these two methods is, arises. According to Booth (1985), the main differences are that weight windows are space-energy-dependent whereas geometry splitting is only dependent on space. When employing geometry splitting, the particle will undergo splitting despite the weight of the particle. With weight windows, it works completely the opposite way; before particles are split or roulette is played, the weight of the particle is checked against the weight window. The geometry splitting method is based on the ratio of importances across the surface. Weight windows are defined by the user in the MCNP input. Although the use of weight windows is more powerful than that of importances, this method requires more input and more insight into the problem. The weight window method is applied at surfaces, collision sites or both. However, the geometry splitting technique is only applied at surfaces.

Another difference between weight windows and geometry splitting is that the weight window can control weight fluctuations introduced by biasing techniques by letting all the particles in a cell adhere to $W_L < W < W_U$. Geometry splitting is weight independent and will preserve any weight fluctuations. To perform splitting the geometry has to be modified, which is not required for the use of weight windows.

2.3.4 Weight cut-off

Weight cut-off is a technique used to kill particles with low weight. To do this, the user supplies a survival weight ($w_{survival}$) and lower weight (w_l). Russian roulette is played if the particle's weight is below the user-specified lower weight and the weight of the survival particles is equal to $w_{survival}$.

Considering a particle with weight w_0, the survival weight and the lower weight, the following holds if the initial weight is less than the lower weight:

$$w_0 < w_l \rightarrow \begin{cases} p = \dfrac{w_0}{w_{survival}} & w' = w_{survival} \\ p^* = 1 - p & w' = 0 \end{cases} \Rightarrow \bar{w}' = p w_{survival} + p^* \times 0 = \frac{w_0}{w_{survival}} w_{survival} = w_0$$

The particle with weight w_0 will either survive with a probability $p = \dfrac{w_0}{w_{survival}}$, in which case the particle is assigned a survival weight $w_{survival}$, or the particle will be cut-off (killed) with probability $1 - p$.

3. Mathematical Derivations

The main goal of Section 3.1 is to state some properties of the adjoint transport equation and operators that contribute to some developments made in this dissertation. In Section 3.2, in particular, it is shown that for a non-multiplicative medium and for a given detector response, the adjoint flux in a phase space point can be interpreted as the importance of such a point to the detector response (Lewis and Miller (1984)). Section 3.3 introduces an approximation to the source biasing using the adjoint flux. Finally, Section 3.4 shows that if the weight of a particle is inversely proportional to the importance of the phase space where the particle is located, then the variance is reduced in a Monte Carlo calculation (Wagner and Haghighat (2003)).

3.1 Adjoint Transport Operator

For completeness this section includes the form of the adjoint transport operator in as introduced in Lewis and Miller (1984).

For non-multiplying systems, the time-independent transport equation is:

$$[\hat{\Omega}\cdot\vec{\nabla}+\sigma(\mathbf{r},E)]\psi(\mathbf{r},\hat{\Omega},E)=q_{ex}(\mathbf{r},\hat{\Omega},E)+\int dE'\int d\hat{\Omega}'\sigma_s(\mathbf{r},E'\to E,\hat{\Omega}'\bullet\hat{\Omega})\psi(\mathbf{r},\hat{\Omega}',E')$$

(3.1.1)

where ψ is the angular flux, $\hat{\Omega}$ is the direction, $\mathbf{r}$ is the position vector, σ is the total macroscopic cross-section, σ_s is the scattering cross-section, E is energy and q_{ex} is the external source.

Then the transport operator H can be defined as:

$$H\psi(\mathbf{r},\hat{\Omega},E)=[\hat{\Omega}\cdot\vec{\nabla}+\sigma(\mathbf{r},E)]\psi(\mathbf{r},\hat{\Omega},E)-\int dE'\int d\hat{\Omega}'\sigma_s(\mathbf{r},E'\to E,\hat{\Omega}'\bullet\hat{\Omega})\psi(\mathbf{r},\hat{\Omega}',E')$$

(3.1.2)

The transport equation can also be expressed as

$$H\psi=q, \qquad (3.1.4)$$

q is the particle source, with the following boundary condition imposed:

$$\psi(\mathbf{r},\hat{\Omega},E)=0,\quad \mathbf{r}\in\Gamma,\ \hat{n}\bullet\hat{\Omega}<0\,, \tag{3.1.5}$$

where $\hat{n}$ is the outward normal vector to the surface Γ. This illustrates that no particles enter the spatial domain bounded by Γ, i.e. the incoming flux is zero. This boundary condition is also referred to as the vacuum boundary condition.

The adjoint transport operator is by definition:

$$H^{+}\psi^{+}(\mathbf{r},\hat{\Omega},E)=[-\hat{\Omega}\cdot\vec{\nabla}+\sigma(\mathbf{r},E)]\psi^{+}(\mathbf{r},\hat{\Omega},E)-\int dE'\int d\hat{\Omega}'\sigma_{s}(\mathbf{r},E\rightarrow E',\hat{\Omega}\bullet\hat{\Omega}')\psi^{+}(\mathbf{r},\hat{\Omega}',E') \tag{3.1.6}$$

Let the following boundary condition be applied to the adjoint transport equation:

$$\psi^{+}(\mathbf{r},\hat{\Omega},E)=0,\quad \mathbf{r}\in\Gamma,\ \hat{\Omega}\bullet\hat{n}\geq 0\,. \tag{3.1.7}$$

This boundary condition implies that the outgoing adjoint flux is zero at the boundary of the system and that *neutrons leaking from the system are not important*.
Next it will be shown that H^{+} is the adjoint of H by proving the following identity:

$$\left\langle \psi^{+}H\psi\right\rangle=\left\langle \psi H^{+}\psi^{+}\right\rangle \tag{3.1.8}$$

The notation $\langle\ \rangle$ is used to denote that the expression is integrated over all the variables, $(\mathbf{r},\hat{\Omega},E)$.
In order to prove this identity in equation (3.1.8), consider the following procedure as discussed in detail in Lewis and Miller (1984):
Multiply equation (3.1.2) by $\psi^{+}(\mathbf{r},\hat{\Omega},E)$ to get

$$\psi^{+}(\mathbf{r},\hat{\Omega},E)H\psi(\mathbf{r},\hat{\Omega},E)=\psi^{+}(\mathbf{r},\hat{\Omega},E)$$
$$([\hat{\Omega}\cdot\vec{\nabla}+\sigma(\mathbf{r},E)]\psi(\mathbf{r},\hat{\Omega},E)-\int dE'\int d\hat{\Omega}'\sigma_{s}(\mathbf{r},E'\rightarrow E,\hat{\Omega}'\bullet\hat{\Omega})\psi(\mathbf{r},\hat{\Omega}',E'))$$

and integrate the expression for $\psi^{+}H\psi$ over all the variables

$$\left\langle \psi^+(\mathbf{r},\hat{\Omega},E)H\psi(\mathbf{r},\hat{\Omega},E)\right\rangle = \int dV\int dE\int d\hat{\Omega}\,\psi^+(\mathbf{r},\hat{\Omega},E)([\hat{\Omega}\cdot\vec{\nabla}+\sigma(\mathbf{r},E)]\psi(\mathbf{r},\hat{\Omega},E) - \int dE'\int d\hat{\Omega}'\sigma_s(\mathbf{r},E'\to E,\hat{\Omega}'\bullet\hat{\Omega})\psi(\mathbf{r},\hat{\Omega}',E'))$$

(3.1.9)

Consider the streaming operator given in Equation (3.1.9),

$$\begin{aligned}
&\int dV\int d\hat{\Omega}\int dE\psi^+(\mathbf{r},\hat{\Omega},E)(\hat{\Omega}\cdot\nabla)\psi(\mathbf{r},\hat{\Omega},E)\\
&=\int dV\int d\hat{\Omega}\int dE\psi^+(\mathbf{r},\hat{\Omega},E)(\nabla\cdot\hat{\Omega})\psi(\mathbf{r},\hat{\Omega},E)\\
&=\int dV\int d\hat{\Omega}\int dE\left[\nabla\cdot\left(\hat{\Omega}\psi^+(\mathbf{r},\hat{\Omega},E)\psi(\mathbf{r},\hat{\Omega},E)\right)-\psi(\mathbf{r},\hat{\Omega},E)\nabla\cdot\left(\hat{\Omega}\psi^+(\mathbf{r},\hat{\Omega},E)\right)\right]\\
&=\int d\hat{\Omega}\int dE\int_\Gamma d\Gamma\hat{n}\cdot\hat{\Omega}\psi^+(\mathbf{r},\hat{\Omega},E)\psi(\mathbf{r},\hat{\Omega},E)-\int dV\int d\hat{\Omega}\int dE\psi(\mathbf{r},\hat{\Omega},E)\nabla\cdot\left(\hat{\Omega}\psi^+(\mathbf{r},\hat{\Omega},E)\right)
\end{aligned}$$

(3.1.10)

where Gauss's law has been applied to the volume integral to convert it into a surface integral.

Equation (3.1.10) can be rewritten as follows:

$$\begin{aligned}
&\int d\hat{\Omega}\int dE\int_\Gamma d\Gamma\hat{n}\cdot\hat{\Omega}\psi^+(\mathbf{r},\hat{\Omega},E)\psi(\mathbf{r},\hat{\Omega},E)=\\
&\int dV\int d\hat{\Omega}\int dE\psi^+(\mathbf{r},\hat{\Omega},E)(\hat{\Omega}\cdot\nabla)\psi(\mathbf{r},\hat{\Omega},E)+\int dV\int d\hat{\Omega}\int dE\psi(\mathbf{r},\hat{\Omega},E)\nabla\cdot\left(\hat{\Omega}\psi^+(\mathbf{r},\hat{\Omega},E)\right)
\end{aligned}$$

(3.1.11)

By applying the boundary conditions, equations (3.1.5) and (3.1.7) to equation (3.1.11) we get that

$$\begin{aligned}
&\int d\hat{\Omega}\int dE\int_\Gamma d\Gamma\hat{n}\cdot\hat{\Omega}\psi^+(\mathbf{r},\hat{\Omega},E)\psi(\mathbf{r},\hat{\Omega},E)=0\\
&\therefore\int dV\int d\hat{\Omega}\int dE\psi^+(\mathbf{r},\hat{\Omega},E)(\hat{\Omega}\cdot\nabla)\psi(\mathbf{r},\hat{\Omega},E)=-\int dV\int d\hat{\Omega}\int dE\psi(\mathbf{r},\hat{\Omega},E)\nabla\cdot\left(\hat{\Omega}\psi^+(\mathbf{r},\hat{\Omega},E)\right)
\end{aligned}$$

The collision term does not change since:

$$\psi^+(\mathbf{r},\hat{\Omega},\mathbf{E})\sigma(\mathbf{r},E)\psi(\mathbf{r},\hat{\Omega},\mathbf{E})=\psi(\mathbf{r},\hat{\Omega},\mathbf{E})\sigma(\mathbf{r},E)\psi^+(\mathbf{r},\hat{\Omega},\mathbf{E})$$

Exchanging $\hat{\Omega}'$ with $\hat{\Omega}$ and E with E' and by changing the order of integration, the scattering term can be rewritten as:

$$\int dV \int d\hat{\Omega} \int dE \psi^{+}(\mathbf{r},\hat{\Omega},\mathbf{E}) \int d\hat{\Omega}' \int dE' \sigma_s(\mathbf{r},\mathbf{E}' \to \mathbf{E},\hat{\Omega}' \cdot \hat{\Omega}) \psi(\mathbf{r},\hat{\Omega}',\mathbf{E}')$$
$$= \int dV \int d\hat{\Omega} \int dE \int d\hat{\Omega}' \int dE' \psi^{+}(\mathbf{r},\hat{\Omega},\mathbf{E}) \sigma_s(\mathbf{r},\mathbf{E}' \to \mathbf{E},\hat{\Omega}' \cdot \hat{\Omega}) \psi(\mathbf{r},\hat{\Omega}',\mathbf{E}')$$
$$= \int dV \int d\hat{\Omega}' \int dE' \int d\hat{\Omega} \int dE \psi^{+}(\mathbf{r},\hat{\Omega}',\mathbf{E}') \sigma_s(\mathbf{r},\mathbf{E} \to \mathbf{E}',\hat{\Omega} \cdot \hat{\Omega}') \psi(\mathbf{r},\hat{\Omega},\mathbf{E})$$
$$= \int dV \int d\hat{\Omega} \int dE \psi(\mathbf{r},\hat{\Omega},\mathbf{E}) \int d\hat{\Omega}' \int dE' \sigma_s(\mathbf{r},\mathbf{E} \to \mathbf{E}',\hat{\Omega} \cdot \hat{\Omega}') \psi^{+}(\mathbf{r},\hat{\Omega}',\mathbf{E}')$$

By applying all these steps we get the following:

$$\left\langle \psi^{+} H \psi \right\rangle = \int dV \int d\hat{\Omega} \int dE \psi(\mathbf{r},\hat{\Omega},E) \times$$
$$\left[-\hat{\Omega} \cdot \nabla \psi^{+}(\mathbf{r},\hat{\Omega},E) + \sigma(\mathbf{r},E) \psi^{+}(\mathbf{r},\hat{\Omega},E) - \int dE' \int d\hat{\Omega}' \sigma_s(\mathbf{r},E \to E',\hat{\Omega} \cdot \hat{\Omega}') \psi^{+}(\mathbf{r},\hat{\Omega}',E') \right]$$
$$= \left\langle \psi H^{+} \psi^{+} \right\rangle \tag{3.1.12}$$

This proves that

$$\left\langle \psi^{+} H \psi \right\rangle = \left\langle \psi H^{+} \psi^{+} \right\rangle .$$

3.2 Interpretation of the Adjoint Flux and Importance

In this section an example is shown to illustrate that the adjoint flux at a given phase space can be interpreted as the importance of such a phase space.

To do this, the calculation shown in Lewis and Miller (1984) where they obtained the response of a small detector to an external source q_{ex} inside a system with a void boundary condition, is reproduced. Let the detector be placed at $\mathbf{r_d}$ with volume V_d and with a total cross section σ_d. Therefore, its response given by the total reaction rate at $\mathbf{r_d}$ is expressed as

$$R = V_d \int dE \sigma_d(E) \phi(\mathbf{r_d},E) \tag{3.2.1}$$

where ϕ is the scalar flux.

The scalar flux can be obtained by solving the neutron transport equation given as equation (3.1.6) with vacuum boundary conditions.

Let the adjoint problem be defined as

$$H^{+}\psi^{+} = \sigma_d V_d \delta(\mathbf{r} - \mathbf{r_d}) , \tag{3.2.2}$$

with the boundary condition given in Section 3.1 for the adjoint flux,

$$\psi^{+}(\mathbf{r}, \hat{\Omega}, E) = 0, \quad \mathbf{r} \in \Gamma, \ \hat{\Omega} \bullet \hat{n} \geq 0$$

If equation (3.1.6) is multiplied by ψ^{+} and integrated over the independent variables, the following equation is obtained:

$$\left\langle \psi^{+} H \psi \right\rangle = \left\langle \psi^{+} q \right\rangle . \tag{3.2.3}$$

In a similar manner, if equation (3.2.2) is multiplied by ψ and integrated over all the variables, it follows that

$$\left\langle \psi H^{+} \psi^{+} \right\rangle = \left\langle \psi \sigma_d V_d \delta(\mathbf{r} - \mathbf{r_d}) \right\rangle = R . \tag{3.2.4}$$

When the difference is taken between (3.2.3) and (3.2.4) the following result is obtained:

$$\left\langle \psi^{+} H \psi \right\rangle - \left\langle \psi H^{+} \psi^{+} \right\rangle = \left\langle \psi^{+} q \right\rangle - R . \tag{3.2.5}$$

From the adjoint identity (equation (3.1.8)) the following is obtained

$$R = \left\langle \psi^{+} q \right\rangle \tag{3.2.6}$$

This result means that the detector response is given by the volume integral of the adjoint flux multiplied by the source distribution. This is a well-known result that is commonly used when solving the transport equation with deterministic methods since once the adjoint flux is calculated for a given detector, it is not necessary to recalculate it to obtain the response at that detector for a different source.
On the other hand, the previous problem provides the physical interpretation of the adjoint flux as the *importance*. If it is assumed that the particles are emitted at $\mathbf{r_0}$ in the direction $\hat{\Omega}_0$ at energy E_0 at a rate of one per second the external source is,

$$q = \delta(\vec{r} - \vec{r}_0)\delta(E - E_0)\delta(\Omega \cdot \hat{\Omega}_0) . \tag{3.2.7}$$

Then the reaction rate obtained is

$$R = \psi^{+}(\mathbf{r}_0, \hat{\Omega}_0, E_0), \tag{3.2.8}$$

which shows that the adjoint flux is the importance of the particle produced at $\mathbf{r}_0, \hat{\Omega}_0, E_0$ to the detector response.

3.3 Source Biasing Equation

Lewis and Miller (1984) define source biasing as the distortion of the distribution of source particles to produce more particles in important regions. Important regions can be referred to as regions where the particles will contribute more to the result (tally).

To determine the source biasing equation the conservation of statistical weight for a source particle, is considered:

$$W(P)\hat{q}(P) = W_0 q(P) \tag{3.3.1}$$

where

$P \in (\mathbf{r}, \Omega, E)$
$W \rightarrow$ Statistical Weight
$\mathrm{W}_0 \rightarrow$ Weight before a variance reduction method is applied
$\hat{q} \rightarrow$ Biased source probability density function
$q \rightarrow$ Source probability density function

This is also referred to as a particle correction formula, which must be introduced whenever physical processes are modified to accurately estimate the physical quantity. The source variables are sampled from the biased probability density function and for this reason it is necessary to adjust the statistical weight of the source with the ratio of the actual probability divided by the biased probability.

Let $W_0 = 1$ in equation (3.3.1). A very important outcome is then obtained which will be used in the rest of this dissertation to determine the source biasing parameters:

$$\begin{aligned} W(P)\hat{q}(P) &= q(P) \\ \hat{q}(P) &= \frac{q(P)}{W(P)} \end{aligned} \tag{3.3.2}$$

To determine the source biasing equation the minimum variance relation must be used. This is proved in Section 3.4:

$$W(P) = \frac{R}{\psi^+(P)}$$

By substituting the relation for a minimum variance and equation (3.2.6) into equation (3.3.2) it follows that the source biasing equation is:

$$\hat{q}(P) = \frac{q(P)\psi^+(P)}{\int_P dP q(P)\psi^+(P)} \tag{3.3.3}$$

It can be seen from equation (3.3.3) that the numerator is the detector response from the element $(d\mathbf{r}, d\hat{\Omega}, dE)$ and the denominator is the total detector response to the source. The denominator is the exact physical quantity that should be determined.

3.4 Statistical Weight Derivation

In this section we want to prove that if the statistical weight of a particle in a region is proportional to the inverse of the importance of a region, then there is an optimization in the variance of the solution of a Monte Carlo calculation. Usually this relationship is either assumed (Conveyou, *et al*. (1967)), or verified by computational analyses. Wagner and Haghighat (2003) made a significant contribution by proving that under certain conditions the previous relation produces zero variance results. Therefore, we will reproduce what was done by Wagner and Haghighat (2003) to show this relationship.

Consider the reaction rate over a phase space P given in equation (3.2.6). From the conservation law of the statistical weight (equation (3.3.2)) and equation (3.3.3):

$$W(P)\hat{q}(P) = q(P)$$

$$W(P)\frac{\psi^{+}(P)q(P)}{\int_{P} dP\psi^{+}(P)q(P)} = q(P) \tag{3.4.1}$$

$$W(P)\frac{\psi^{+}(P)}{\int_{P} dP\psi^{+}(P)q(P)} = 1$$

Then by rewriting equation (3.4.1) the final result is

$$W(P) = \frac{\int_{P} dP\psi^{+}(P)q(P)}{\psi^{+}(P)} = \frac{R}{\psi^{+}(P)}. \tag{3.4.2}$$

Equation (3.4.2) shows that the statistical weight of the particle in a particular region is proportional to the inverse of the importance of that region.

3.5 Summary

This chapter discussed concepts such as the adjoint flux, statistical weight, importance and source biasing. It was shown that the adjoint flux in any phase space point can be interpreted as the importance of such point in the phase.

Another concept derived in this chapter is the relation showing that the statistical weight of the particle in a region is proportional to the inverse of the importance of a region.

Also introduced in this chapter is the approximation to source biasing using the adjoint flux. With this, an alternative probability density function, referred to as a biased probability density function, is defined so that it will lower the variance of the response.

4. Methods and Results

The preceding chapters discussed the concepts of adjoint flux, statistical weight of a particle, importance and source biasing. Variance reduction methods, namely weight windows and geometry splitting, were also introduced. Chapters 4 and 5 illustrate how these concepts and methods can be used to improve the statistics of an MCNP calculation. The cases presented in this chapter outline separate effects, whilst the case presented in the next chapter illustrates a typical test that involves all the above-mentioned concepts. The latter problem uses a graphite cylinder similar to the top part of the bottom reflector of the PBMR.

The three case studies presented in this chapter are:

- An iron cylinder with a source along its axis consisting of four zones with a variation in intensity such that each of these source zones has the same contribution to the tally situated in an annulus at the bottom of the cylinder. The main goal of this case study is to look into the procedure on how to determine weight windows for a high absorbent photon medium (Section 4.1.1), and to show how the convergence of the MCNP calculation is improved when using weight windows and source biasing consistent with weight windows. The case study consists of a large source where the important and less important regions contribute equally to the tally. This property of the system is used to show the necessity of biasing the photon source when using weight windows as a variance reduction method. This is done in order to prevent unnecessary calculations due to particles that are born with weights far from the weight windows bounds. In other words, in order to have meaningful results and to reduce the computational time of the calculation, it is necessary to bias the source so that the source particles are born inside the weight window bounds. Section 4.1.2 gives a description on how to use weight windows to determine the source biasing parameters. The case study is done for three scenarios, namely with no weight windows, with weight windows, and with source biasing consistent with weight windows (Section 4.1.3). It is shown that optimal results are obtained when the source particles are born inside the weight window bounds.

- After observing the improvements that can be obtained in the Monte Carlo efficiency using weight windows and source biasing in the first case study, the second case study, presented in Section 4.2, is performed to analyse the effect on the statistics of the results when the source region is partially biased. The motivation for considering this case study is because there are configurations where it is not possible to bias all the variables of the source particles so that they are born inside the weight window bounds. The system solved is the same as in the previous case but the photon source is divided in two zones; one, which is more important, and a second zone, which has a higher contribution to the tally. The same weight windows generated in Section 4.1.1 are used in this case study, but instead of using them to bias the source, as done in the previous case study, the weight windows are just scaled up or down to bias either zone 1 or zone 2 of the photon source. The main conclusion drawn from this analysis is that for this particular case, it is more advantageous to bias the zone with higher contribution to the tally than to bias the more important region. This case study does not present a general solution to all these types of problems. It should be considered as a word of warning to MCNP users to outline the importance of investigating how the source should be biased before solving major problems with the Monte Carlo method. The results for the corresponding analysis are presented in Section 4.2.
- The third case study introduced in Section 4.3 investigates a coupled neutron-photon problem. The main objective is to generate weight windows for a photon tally when running a coupled neutron-photon problem and to show how these weight windows can be used in a photon problem on its own. This methodology to generate weight windows is based on the fact that the importance function is dependent on the tally and independent of the source (see Chapter 3). The obvious limitation is that for both the coupled neutron-photon and the photon problem the same photon tally must be used. It should be noted that this methodology is less efficient when the materials involved have low photon production cross sections. In particular, it should not be applied to materials that are *transparent* for neutrons. This methodology is investigated for two scenarios. Both these scenarios consist of high photon production cross-sections through neutron reactions.

4.1 Case Study 1

This case study consists of an iron cylinder, with a radius of 10 cm and height of 29 cm, containing a 3 cm radius cylindrical source as shown in Figure 6. This 3 cm cylinder is filled with cobalt material. The average scalar photon flux is calculated at the lower surface of the system inside the annulus between 7 cm and 10 cm radius with a height of 1.3 cm.

The source is axially divided into four zones. The axial intensity[3] distribution of the source is defined so that the four source zones have similar contributions to the average scalar photon flux at the tally region. Defining the intensity of zone 1 as $I_1 = 1$ particles/sec, the intensities for zones two, three and four are $I_2^* = 47$ particles/sec, $I_3^* = 4E+03$ particles/sec and $I_4^* = 3E+04$ particles/sec respectively.

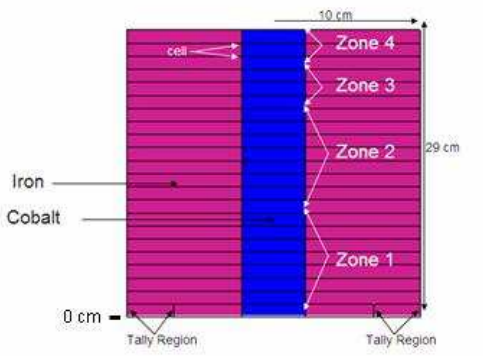

Figure 6: Vertical Section of the Cylindrical System for Case Study 1

The main objectives of this case study are to introduce one methodology to determine weight windows for this system and to show how the convergence of the MCNP calculation can be improved when applying weight windows.

The iron cylinder is a highly absorbent material for photons and for this reason variance reduction methods are needed when evaluating the photon flux for this system.

[3] The intensity of the source is described as the amount of particles per second being emitted from the source.

The next section gives a procedure describing how weight windows were generated with MCNP using geometry truncation and ring detectors. The weight windows generated are also used to determine a biased source probability density function that guarantees that the weights of the source particles for this case are within the weight window bounds.

In order to see how the use of variance reduction methods improves the statistics of an MCNP calculation, comparisons are done using no weight windows, using only weight windows, and using source biasing consistent with weight windows. This is presented in Section 4.1.3.

In many cases it is not possible to bias the source so that all the source particles are within the weight window bounds. For this reason, cases where the source particles are born above and below the weight window bounds are compared to determine which one improves the statistics of the results. It will therefore be shown in Section 4.1.3 that the position of the source particles relative to the weight window bounds has an influence on the statistics of the MCNP result.

4.1.1 Weight Window Generation

The weight windows generator of MCNP has been used to determine weight windows for the current case study. When generating weight windows, it is easy to generate unwanted zeros. Zero weight windows in a cell are either due to particles not entering that cell, or due to particles that did enter the cell but did not add to the tally score (or to their daughters) - see Equation (2.2.2). To increase the number of particles that enter (or that are born in) the cells of the system, a uniformly distributed volumetric photon source that covers the whole system is used. A ring detector is used to increase the number of particles tallied.

The whole system above the ring detector is filled with the uniform volumetric source. During each step the radius of the ring detector is gradually increased (see Figure 7) and the source is axially extended up to the position of the ring detector. The radius of the initial ring detector is taken as similar to the radius of the source and the radius of the last ring detector as equal to the radius of the iron cylinder. The reason for doing this is to avoid zero weight windows in the source region since

these weight windows are used to bias the source. The detector is moved in small intervals. Each new interval is considered to be a new iteration. During each iteration, new weight windows are generated in a new MCNP run using as variance reduction the previously-calculated weight windows.

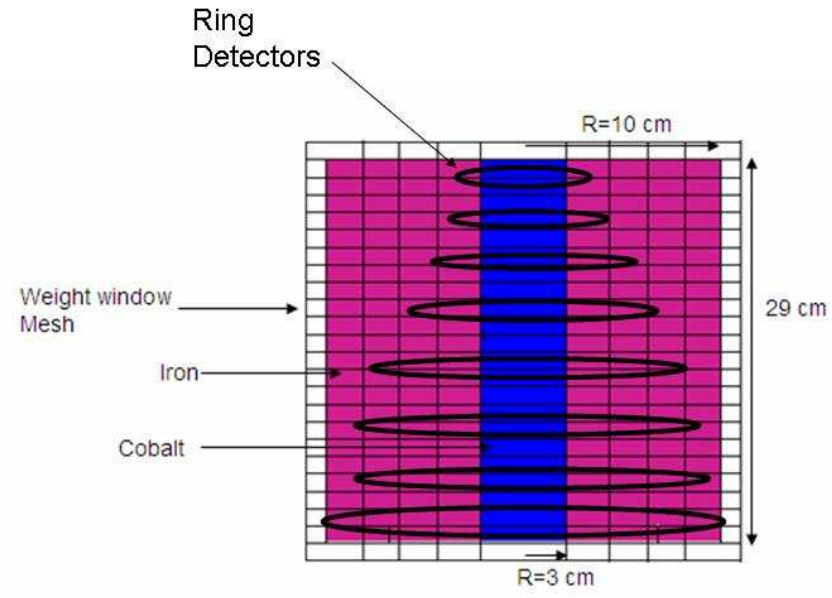

Figure 7: Position of Ring Detectors

To save computational time the part of the geometry just below the ring detector is truncated. When truncating the system, no calculation time is spent following the history of a particle not important to the tally. The whole domain will have been considered by the time the iterative process has been completed.

The first two steps for generating weight windows as outlined above are presented in more detail. Consider the first one[4] centimetre of the top part of the system – and, in so doing, truncate the rest of the system. Fill this 'one-centimetre high cylinder' with a volumetric source covering the whole cylindrical system. A ring detector with a three-centimetre radius is positioned at the bottom of this one-centimetre cylinder. Weight windows can now be generated for this one centimetre cylinder. This completes the definition of the weight windows for the top one centimetre of the system.

[4] Note that the dimensions and distances used are applicable to this specific case. They will be different for different cases.

For the second iteration the cylindrical system should be extended a further two centimetres axially and rest of the system should be truncated. Fill this three-centimetre cylinder with a uniform volumetric source. Position the point detector at the bottom of this cylinder and extend the radius of the point detector with another centimetre. At this stage weight windows can be generated for this three-centimetre cylinder (the remainder of the geometry below the ring detector has been truncated). This set of weight windows are based on the weight windows generated for the one-centimetre cylinder. Therefore, by 'reading' the previous weight windows a set of good importance estimates can be produced for the three-centimetre cylinder. This procedure must be continued up to the lower surface of the original cylinder.

It is important to note that when using a set of weight windows to perform an MCNP calculation; the set must be scaled using a user-defined scaling factor. A reference point with a user-defined normalization factor can also be specified in order to make the cell containing the reference point have the specified value. These two parameters, scaling factor and reference point with normalization factor, must be analysed in every iteration in order to have the weights of most of the source particles within the weight windows limits.

In summary, throughout the process of generating weight windows with the MCNP generator, one should continuously verify the statistical information of the MCNP run, especially the relative error and FOM. The mesh size of the superimposed weight windows mesh has an influence on the efficiency of the results. Large mesh sizes can cause high weight ratios between adjacent cells, which could produce over-splitting causing the MCNP run to hang. A too-fine mesh can cause unnecessary calculations that do not contribute directly to the quality of the solution and are expensive with regard to calculation time. Therefore, it is important to choose the correct mesh size. In general, an improvement was observed in the statistics of the result if the ratio of importances between adjacent cells is not greater than a factor of ten. It also often helps to check whether the normalization factor lies within the more important cell. If the iterative process described does not create convergence, the ring detector should be moved in smaller increments or the superimposed mesh should be modified.

4.1.2 Source Biasing consistent with Weight Windows

This section discusses how the source is biased consistent with the weight windows obtained in Section 4.1.1.

To do source biasing, a biased source probability density function $\hat{q}_i(\mathbf{r})$ ($particle/cm^3-\sec$) is defined according to Equation (4.1.1). By using this formulation the weights of the source particles are changed to have the same behaviour as the weight windows within the source region. Using a scaling factor puts the biased weights of the source particles within the one-group energy weight window bounds. As shown in Chapter 3, the biased source probability density function is equal to:

$$\hat{q}_i(\mathbf{z}) = \frac{q_i(\mathbf{z})}{W_i(\mathbf{z})} = \frac{\left[\frac{I_i(\mathbf{z})}{Vol_i(\mathbf{z})}\right]}{W_i(\mathbf{z})} \tag{4.1.1}$$

where the index i corresponds to a cell in the source region, $q_i(\mathbf{z})$ is the real source probability density function, $W_i(\mathbf{z})$ is the lower weight windows bound, $Vol_i(\mathbf{z})$ is the volume and $I_i(\mathbf{z})$ is the intensity of the source in the cell i.

Figure 8 shows the weights of the source particles together with the weight windows bounds at the source region. The case identified as only weight windows corresponds to a unit weight for the source particles and the weight windows without any scaling factor. It can be seen that, in this case, almost all the source particles are below the weight windows bounds and only part of the weights of the source are within the weight window bounds. In the rest of the cases shown in Figure 8, the source has been biased consistent with the weight windows as described in the previous paragraphs. In these cases, different scaling factors are applied to the weight windows to have the weights of the source particles born below, inside or above the weight windows bounds,

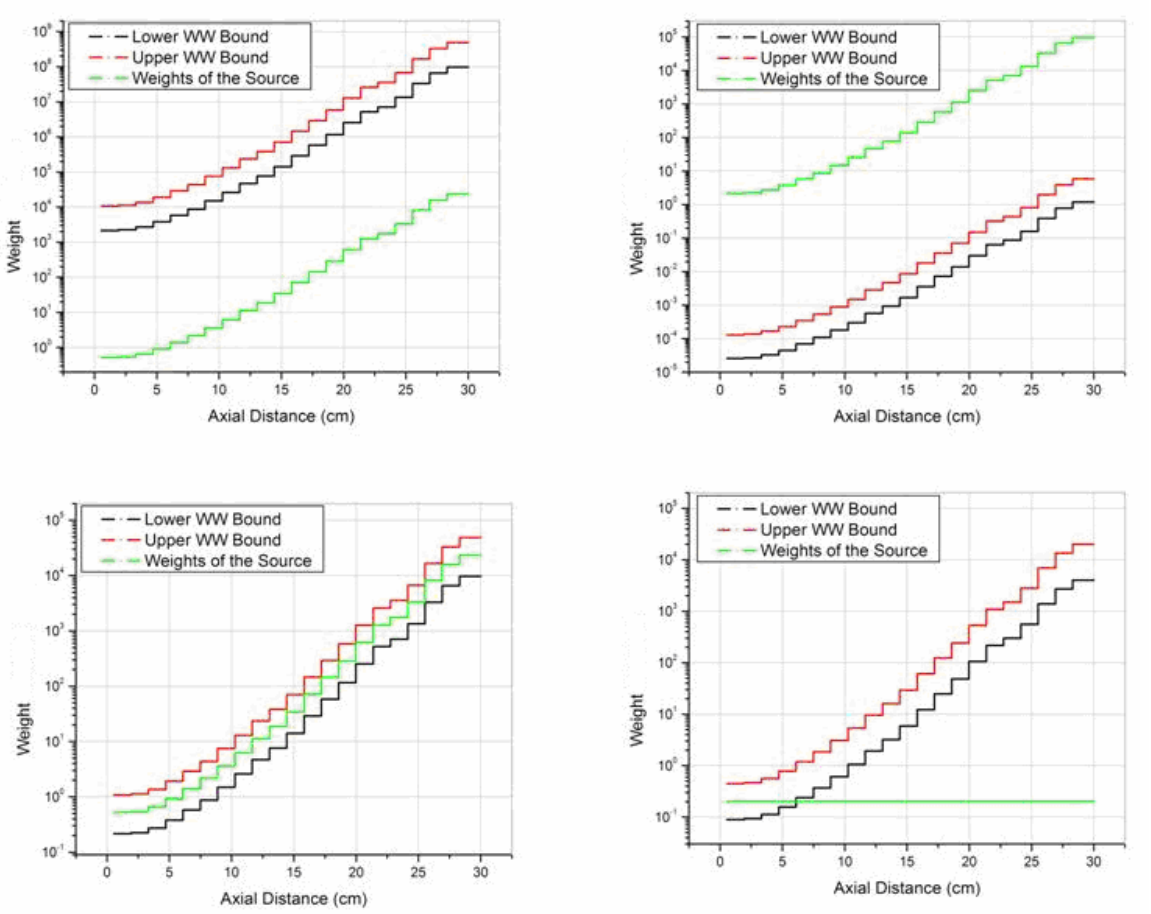

Figure 8: Weight Window Bounds and Weights of Source Particles.

From Figure 8 it can be noted that the weight windows' values increase when increasing the distance to the tally region. This is in accordance with the use of weights inversely proportional to the importance.

4.1.3 Results for Case Study 1

The problem is solved for different scenarios with the intensity distribution for the source and the weight windows that was obtained.

To show the enhancement in the convergence of an MCNP calculation, scenarios such as calculating the flux with and without weight windows and calculating the flux by means of source biasing consistent with weight windows are compared. Examples are also shown that analyse the behaviour of the statistical errors when all the source particles are born above or below the weight window bounds.

For all these cases, the average scalar photon flux is calculated at the lower surface of the system, inside the annulus between the radii of 7 cm and 10 cm, with a height of 1.3 cm - see Figure 6.

Table 2 shows the results obtained for case study 1 after running 2E+07 particles in MCNP. Not all the statistical indicators provided in the MCNP output are investigated for this case. Only the tally mean value, relative error and FOM are considered since these indicators show if there is improvement when applying the different variance reduction techniques.

It can be seen that the best statistics are obtained when all the weights of the source particles are within the weight windows bounds.

Since it is not always possible to have the weights of all the source particles inside the weight window bounds, two extreme cases were analysed where all the source particles are below or above the weight window bounds. As shown in Table 2, in the current problem, it is better that all the source particles are born inside the weight window bounds. The FOM is higher and the relative error smaller compared to the case where all the source particles are born below or above the weight window bounds. Splitting occurs where all the weights of source particles are above the weigh window bounds and Russian roulette occurs where all the weights of the source particles are below the weight window bounds. The number of histories run for the case where all the source particles have weights above the weight window bounds are 2E+06 particles. This is because the case runs for a very long time compared to the other cases. According to the MCNP user manual (Booth, *et al*. (2003)), splitting causes the sample history variance to decrease and the calculation time to increase, whereas Russian roulette causes the sample history variance to increase and the calculation time to decrease. Therefore, even though the sample history variance has decreased when splitting occurs, the FOM will be less if compared to the other cases because of the extremely long calculation time. Where all the source particles have weights below the weight window bounds the relative error is high compared to the other cases.

Table 2: The Results for Case Study 1.

Scenario	Tally Mean ($\gamma / cm^2 - \sec$)	Relative Error	FOM
No Weight Windows	3.6E-08	0.1	2.9
Only Weight Windows	4.1E-08	0.1	10
Source Biasing consistent with WW (weight of source particles within WW bound)	3.18E-08	0.002	3952
Source Biasing consistent with WW (weight of source particles below WW bound)	3.2E-08	0.1	12
Source Biasing consistent with WW (weight of source particles above WW bound)	3.18E-08	0.002	10.0

4.2 Case Study 2

The aim of this case study is to analyse whether it is more efficient to bias the source in high importance regions with low contribution to a tally or in less important regions with high contributions to the tally.

The system used is the same as in the previous case, see Figure 6. The only difference is that in the current case the source is divided into only two zones of different intensity instead of into four zones. The more important zone, closer to the tally region, has lower intensity than the less important one so that the less important zone contributes more to the tally. The tally for this case is the same as the tally defined in Section 4.1, which is the average scalar photon flux at the lower surface of the system inside the annulus between the radii of 7 cm and 10 cm with a height of 1.3 cm.

Due to the very general definitions that a source can have in MCNP, it is not always possible to bias all the variables that define the source in an MCNP calculation. Although this is not the case in the current case study, the intention is to analyse in a simplified problem, the effects of different biasing schemes on a complex source.

However, it is important to note that, regardless of the conclusions of this case study, it is always possible to split the problem into more than one run, each with disjoint partial sources. Therefore, the conclusions of this case study can be considered as another option to be applied when the sources for MCNP are defined.

Figure 9 illustrates the source zones, where the intensities of zones 1 and 2 are equal to 1 and 10^7 photons per second, respectively.

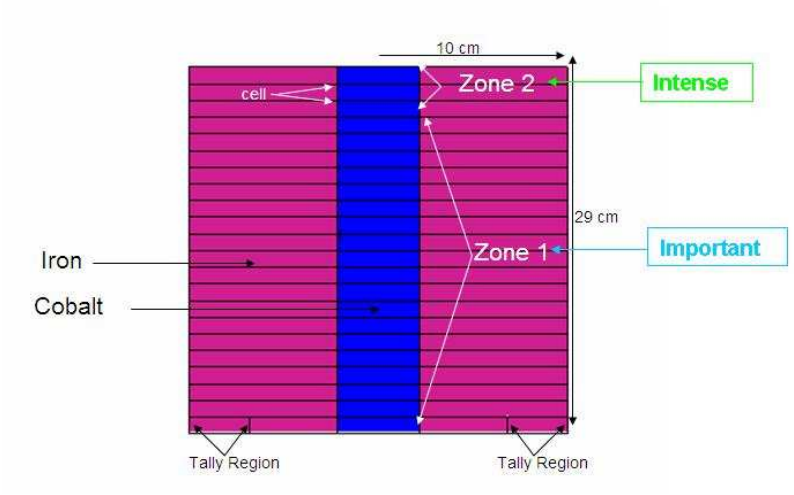

Figure 9: Vertical Section of the Cylindrical System for Case Study 2

In order to calculate the response to the tally from each zone the problem is split into two parts. Firstly, only the source in zone 1 with an intensity of one photon per second is considered. The calculated contribution to the tally in this case is 5.9E-05 $\gamma/cm^2-\sec$ with a relative error of 0.01. Secondly, the problem is solved with the source in zone 2 equal to 10^7 photons per second and no source in zone 1. The calculated contribution to the tally from zone 2 only is 4.87E-02 $\gamma/cm^2-\sec$, with a relative error of 0.005.

The previous results were used to define a photon source for the entire problem with unit total intensity and emission probabilities equal to $1/\left(19+3\times10^7\right)$ in each of the 19 regions of zone 1 and $10^7/\left(19+3\times10^7\right)$ for each of the three regions of zone 2.

The weight windows generated for the previous case study are used in the current one. The reason for being able to use the same weight windows is because the

geometry and materials of the system as well as the definition of the scalar average flux tally in both case studies is the same. This is valid because it was proved in Chapter 3 that the importance function is independent of the source and only dependent on the tally.

Below is a detailed description of the methodology followed by how this type of problem was investigated. The two source scenarios used and detailed in Figure 10, are the following:

- **Scenario 1**: The source is biased so that the particles born in the region contributing more to the tally have weight within the weight window bounds. The rest of the source particles have weight below the weight window bounds.
- **Scenario 2**: The source is biased so that the particles born in the more important part of the source have weight within the weight window bounds. The rest of the source particles have weight above the weight window bounds.

For both these scenarios the source is biased so that the biased probability of emission of the source in the more important region is 82% and in the region contributing more to the tally it is 18%.

In Figure 10 the weight windows are given as a function of the axial distance to the bottom of the iron cylinder. The solid green line is the biased weight of the source particles, the black line is the lower weight window bound, and the red line is the upper weight window bound.

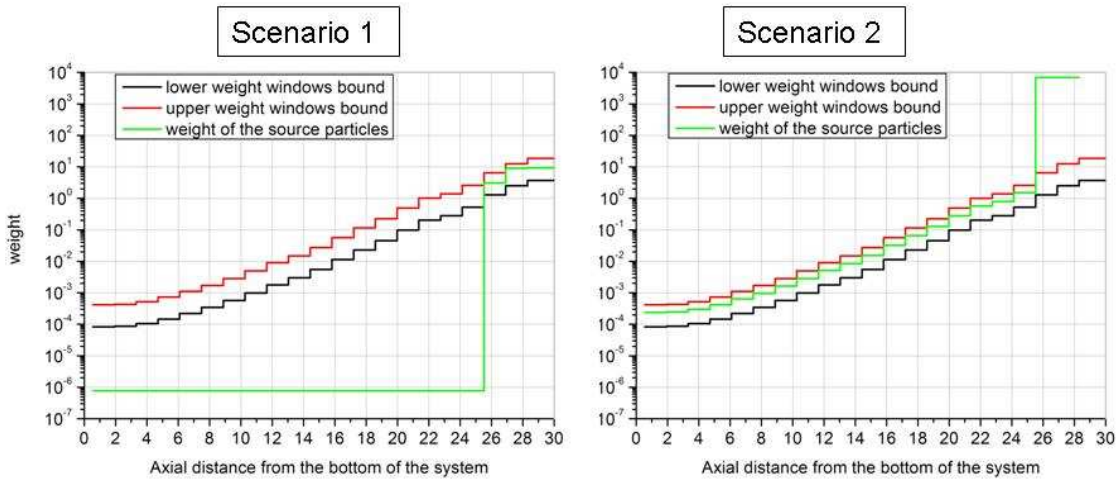

Figure 10: (a) Scenario 1. (b) Scenario 2.

4.2.1 Results for Case Study 2

The number of histories run for Scenario 1 is 1E+06 particles. The calculation time for this run is only two minutes. However, the number of histories run for Scenario 2 is only 1.8E+04 particles and the calculation time is two hours. For both cases all the statistical checks have passed, which indicates that both cases have converged. Comparing the results for the tally and the statistic indicators given in Table 3 for both Scenario 1 and 2, it is evident that Scenario 1 is more efficient. The reason for the low efficiency in Scenario 2 could be due to the fact that the source particles undergo splitting when they are born with weights above the weight windows. The tally mean values for both scenarios are nearly the same. Both these values fall within each other's error bars.

Table 3: Biasing the Intense Part vs the Important Part

Scenario	Tally Mean ($\gamma / cm^2 - \sec$)	Relative Error	FOM
Scenario 1	4.9E-09	0.03	829
Scenario 2	5.0E-09	0.08	1.6

Therefore, it can be concluded that more efficient results can be obtained if the source is biased so that part of the source particles has weight within the weight window bounds in the region contributing more to the tally. For this particular case, the rest of the source particles must have weight below the weight window bounds and be in the region with the higher source emission probability. This is the region where the weights of the source particles will mostly undergo Russian roulette.

4.3 Case Study 3

This case study aims to illustrate when weight windows generated for a photon tally in a coupled neutron-photon problem with an external neutron source can be used in a photon transport problem. The following two scenarios are considered:

- An iron cylinder with a radius of 75.4 cm and a height of 30 cm
- A heavy concrete cylinder with a radius of 200 cm and a height of 150 cm

The rationale behind the selection of these two cases is that both cases have high photon production cross-sections through neutron reactions. By defining a coupled neutron-photon problem with a neutron source it is therefore possible to tally photons and to obtain weight windows for photons which can be used for further analysis in a photon-only problem.

The iron system contains a neutron surface source at the top of the system. This neutron source is uniformly distributed through the entire top surface and is defined by a 2 MeV downward neutron current. A downward photon current tally is defined at the lower surface of the system inside the annulus between the 20 cm and 50 cm radii.

The heavy concrete cylinder consists of a neutron surface source positioned at the top of the system. This source is distributed uniformly through the entire top surface. The neutron source is defined by a 2 MeV downward current. Photons are tallied in a ring detector of 40 cm radius located at the lower surface of the system.

4.3.1 Weight Window Generation for the Coupled Neutron-Photon case

The generation of the one-group energy weight windows for the coupled neutron-photon cases described previously are discussed here.

To begin with, weight window generation for the iron cylinder is discussed. The methodology used was to run the automatic weight windows generator of MCNP in the system with a proper importance distribution for splitting and Russian roulette. Due to the relatively small dimensions of this system, the weight windows were generated in only one MCNP run meaning that geometry splitting and Russian roulette worked properly as variance reduction for this problem.

The tally used is the downward surface photon current positioned in the annulus between the 20 cm and 50 cm radii at the bottom of the system.

Using geometry splitting with Russian roulette to generate weight windows is not always advisable. To perform splitting the geometry has to be modified, which is not required for the use of weight windows. Another disadvantage of using geometry splitting and Russian roulette to generate weight windows is when the weight windows file is read, the importances of all the cells are set to one, which means that geometry splitting can only be used for the first iteration in the process.

For example, when considering the heavy concrete case, due to the high dimensions of this system, the use of splitting with Russian roulette was not enough to generate appropriate weight windows. For this reason the procedure discussed in Section 4.1.1 was used. This procedure entails moving a ring detector from the position of the source up to the position of the real tally. A ring detector with a radius of 40 cm was the tally used in the weight windows generation process. At the end of the process, to generate the final set of weight windows, the ring detector was replaced with the real tally, which is the downward photon current in the annulus between radii 20 cm and 50 cm.

Although the coupled neutron-photon case was used to generate weight windows for the photon case, some analysis of the results obtained for this coupled case are presented here which are summarized in Table 4 and Table 5.

The number of histories run for the iron case is 1.2E+07 particles. In this case, the results reported in Table 4 are converged as they pass all the 10 convergence checks performed by MCNP. It can be seen that there is an improvement in the FOM when using geometry splitting and weight windows compared to the case with no variance reduction.

For the heavy concrete case, Table 5 shows that without using variance reduction techniques, no particles are tallied. The converged results when using weight windows are also given here. The number of histories run for the extended heavy concrete case is 1.9E+06 particles.

Table 4: Iron Cylinder: Results for the Coupled Neutron-photon Case

Scenario	Tally Mean ($\gamma / cm^2 - \sec$)	Relative Error	FOM
No Weight Windows	1.27E-03	0.009	768
Geometry Splitting	1.28E-03	0.006	1078
Weight Windows	1.27E-03	0.006	1427

Table 5: Heavy Concrete Cylinder: Results for the Coupled Neutron-photon Case

Scenario	Tally Mean ($\gamma / cm^2 - \sec$)	Relative Error	FOM
No Weight Windows	0	0	0
-Weight Windows	3.10E-11	0.006	7.8

Figure 11 presents the photon distribution obtained for the iron-coupled neutron-photon case within the annulus $45 \le R \le 55$ cm. It can be seen that the photons are

quite well-distributed throughout the system. To conclude, this photon source is a good candidate for generating photon weight windows.

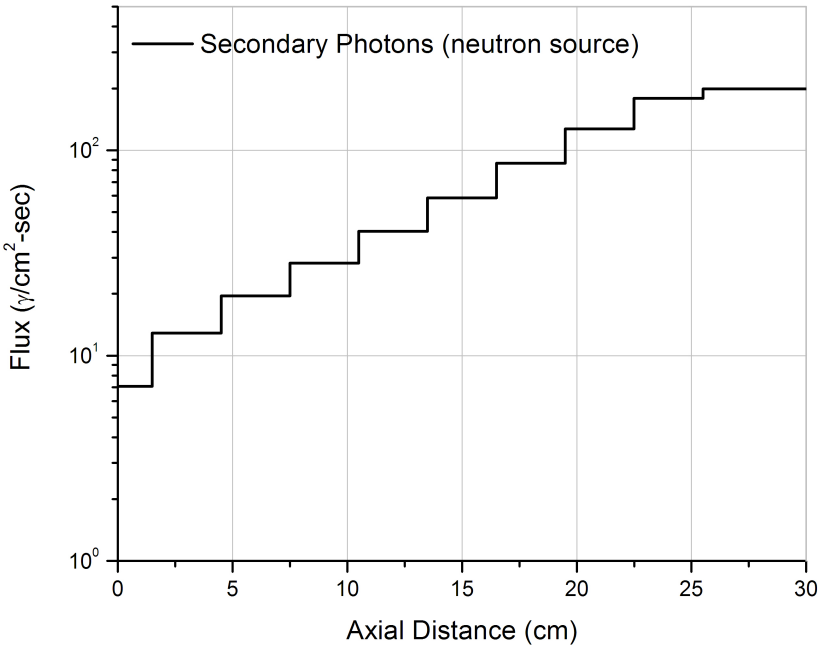

Figure 11: Axial Photon Flux Distribution in the Coupled (n,p) Problem for the Iron Case

Similar conclusions are obtained for the heavy concrete case where Figure 12 shows the axial photon distribution within the radial interval $30 \le R \le 50$ cm.

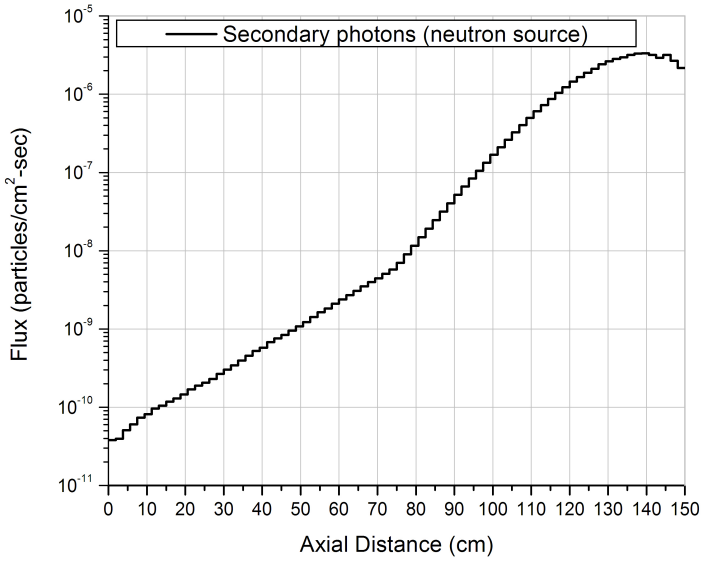

Figure 12: Axial Photon Flux Distribution in the Coupled (n,p) Problem for the Heavy Concrete case

4.3.2 Results for the Photon Case

The photon iron system contains a photon source that is distributed uniformly isotropic through the entire top surface. It is defined by a 1 MeV downward photon current source. The geometry and the tally are kept the same for the iron cylinder case, as defined in the previous section.

For the heavy concrete photon case a photon source is defined as being uniformly distributed through the entire top surface. This photon source is a 2 MeV downward photon current source. As with the previous case the geometry and the tally are kept the same.

Figure 13 presents the weight windows used for the iron case at the upper surface of the system. It shows how the weights of the photon source particles are biased to be within the weight window bounds. The solid black lines are the weights of the source particles, the green lines are the upper weight window bound and the red lines the lower weight window bound. It can be seen that the minimum weights occur around the annulus of the tally which is in accordance with the inverse proportionality between importance of a region with statistical weight of the particles in such region.

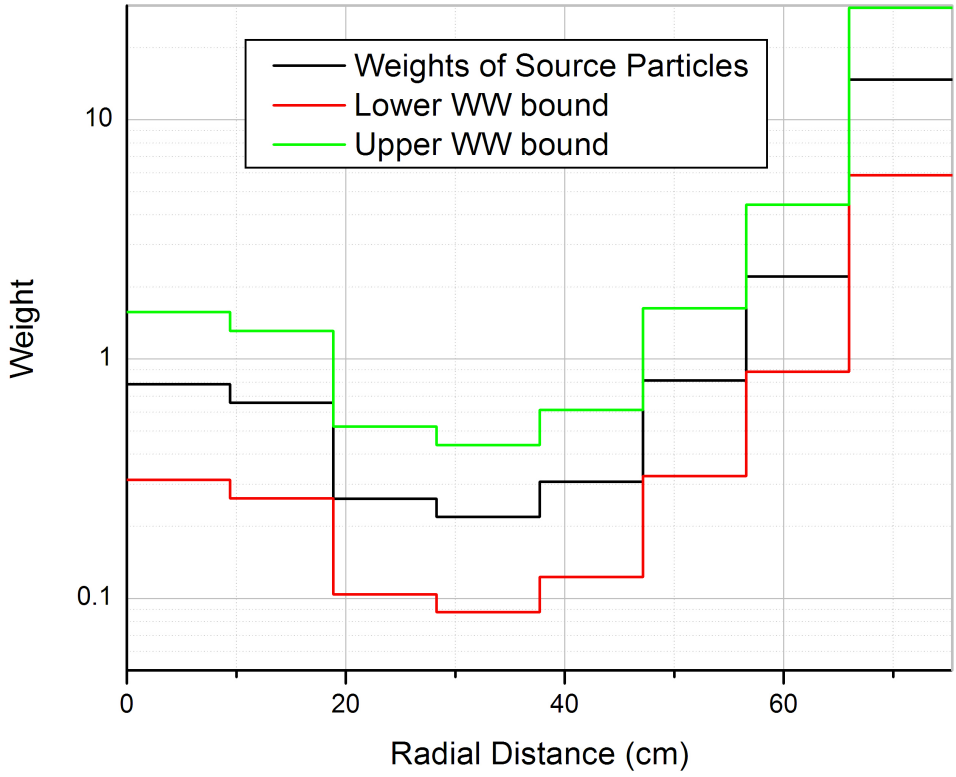

Figure 13: Source Biasing consistent with Weight Windows for the Iron Case

The results for the tally mean, FOM and relative error for the iron photon case are presented in Table 6. Two scenarios are considered. Both these scenarios were run for 2E+07 particles in MCNP.

The first scenario given in Table 6 is the case without any weight windows, which has not converged. On the other hand, for the second scenario, which is the iron photon case with weight windows and source biasing, all the convergence tests have passed. When comparing the two scenarios it is clear that Scenario 2 has a higher FOM than Scenario 1. This indicates that Scenario 2 is more efficient.

This case illustrates that the weight windows generated for the coupled neutron-photon problem can successfully be used for photon problems.

Table 6: Results for the Iron Cylinder Photon Case

Scenario	Tally Mean ($\gamma / cm^2 - \sec$)	Relative Error	FOM
No Weight Windows	6E-07	0.3	1.3
Source biasing consistent with Weight Windows	6.97E-07	0.008	640

Figure 14 presents the weight windows used at the upper surface of the heavy concrete case, as well as the biased photon source. The solid red line is for the lower weight window bound, the black line represents the weights of the source particles and the green line is for the upper weight window bound. The minimum weight occurs in the region of the ring detector, between $0 \le R \le 40$. The non-monotonic behaviour of the weight windows in the outer domain of the cylinder is due to a lack of convergence. It was observed that this lack of convergence does not significantly affect the efficiency of the calculations.

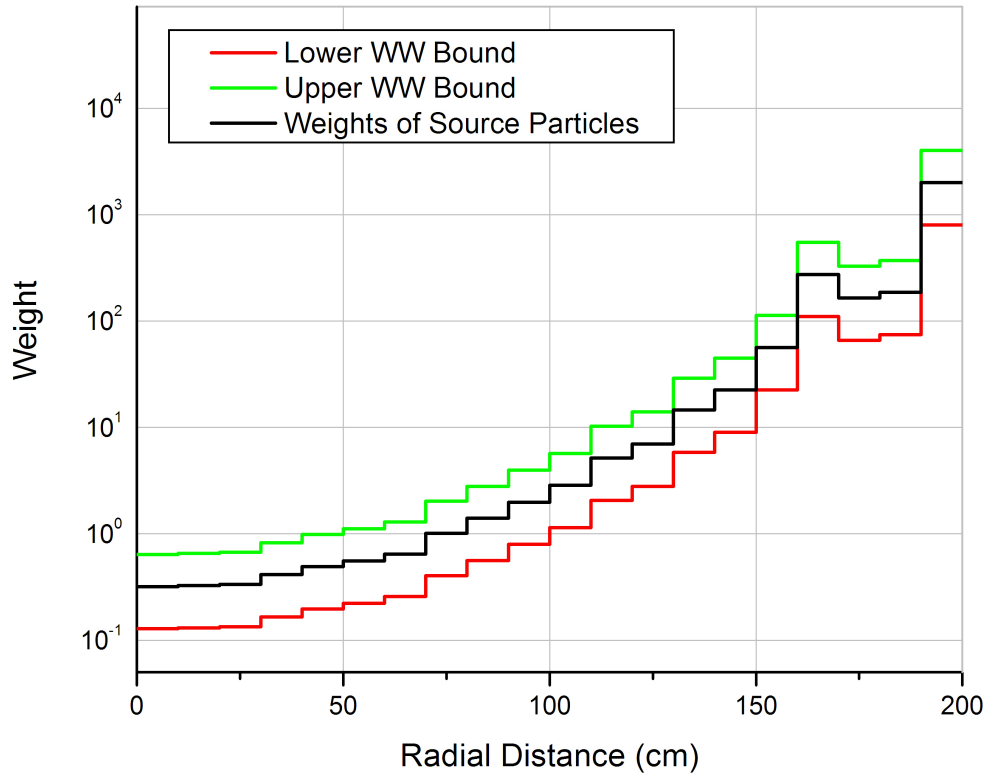

Figure 14: Source Biasing Consistent with Weight Windows for the Heavy Concrete Case

Table 7 gives the results for the tally mean, FOM and relative error obtained after 2E+07 histories. As in the previous case two scenarios are considered. The first scenario is the heavy concrete photon case without any weight windows. The second scenario is the heavy concrete photon case with weight windows and source biasing.

In Scenario 1 the tally did not converge, whereas for Scenario 2 all the statistical indicators have passed. When comparing the two scenarios it is clear that Scenario 2 has a higher FOM than Scenario 1. This indicates that Scenario 2 is more efficient.

Table 7: Results for the Heavy Concrete Cylinder Photon Case

Scenario	**Tally Mean** ($\gamma / cm^2 - \sec$)	**Relative Error**	**FOM**
No Weight Windows	9E-08	0.7	3.9E-02
Source biasing consistent with Weight Windows	8.92E-08	0.007	87

It can therefore be concluded that it is possible to use weight windows generated for a photon tally in a coupled neutron-photon problem with an external neutron source for a photon transport problem.

4.3.3 Summary

Two cases were presented in this study namely, an iron cylinder and a heavy concrete cylinder. Both these cases have high photon production cross-sections through neutron reactions. This study has shown that by defining a coupled neutron-photon problem with a neutron source it is possible to obtain weight windows for photons that can be used for further analysis in photon-only problems. It should be kept in mind that this methodology is less efficient when the materials involved have low photon production cross sections.

5. The Graphite System

This chapter introduces a problem to show how weight windows and source biasing consistent with weight windows can be applied to a system similar to the PBMR bottom reflector.

The PBMR has a centre, side, top and bottom reflector. The bottom reflector forms three cones that channel the fuel elements into three defuelling chutes from where they can be re-circulated to enter the core through the top reflector (Prinsloo (2006)). These defuelling chutes are equally spaced in the centre of the fuel annulus. The radius of the defuelling chute is 25.5 cm. The fuel pebbles will move through the defuelling chutes and at the bottom of these chutes a mechanism will extract the fuel. Burn-up and fuel integrity are then checked. When the measurements are complete the fuel will either be re-circulated or discarded to the spent fuel storage tanks. Figure 15 shows the PBMR bottom reflector, which is positioned below the core and contains three defuelling chutes.

The bottom reflector contains graphite material, three penetrations made up of the primary two inlet connections and one outlet connection, a gas plenum and flow slots. It has a radius of 275 cm and a height of approximately 470 cm. What makes the shielding analysis of the PBMR bottom reflector complex is the height of the system, fissions that occur along with the slowing down process, and void volumes in the system. The Helium enters the reactor via the primary inlet plenum. The main flow path of the helium is then along the vertical riser channels situated in the side reflector, to the inlet slots at the top of the reactor. From the inlet slots the helium fills the void above the pebble bed and then flows through the pebble bed to the outlet slots. Flow slots channel the gas from the bottom of the core to the outlet plenum. The function of the outlet plenum is to distribute and accumulate the coolant gas. From the outlet plenum the hot gas exits the reactor at the outlet duct. The outlet slots, outlet plenum and hot gas duct are all referred to as void volumes.

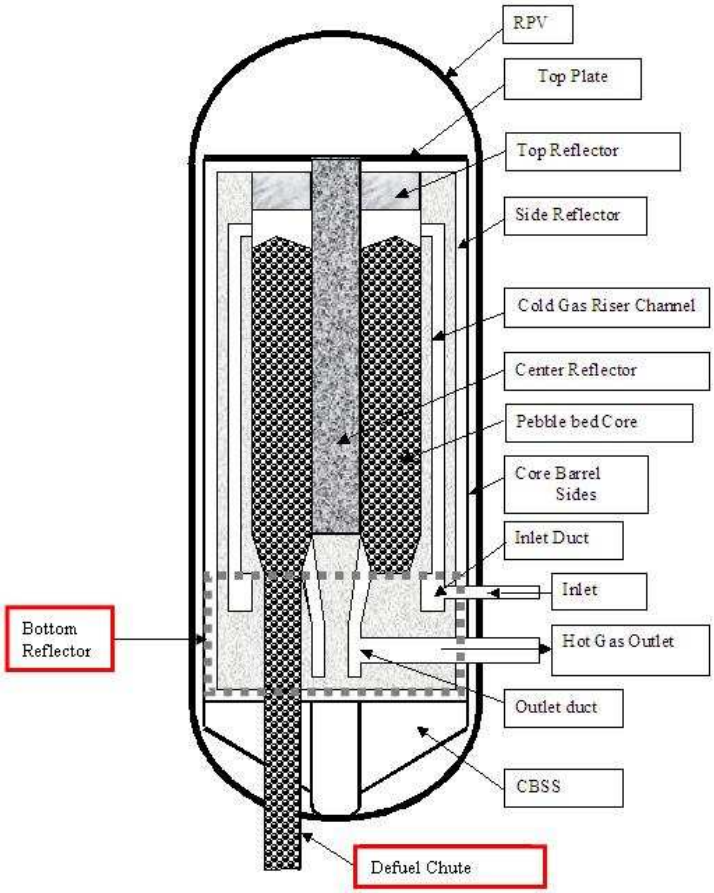

Figure 15: Vertical section of PBMR Bottom Reflector and Defuelling Chutes (Koster (2008))

The case to be analysed is a graphite cylinder with a radius of 275 cm, a density of 1.80 g/cm^3 and a height of approximately one metre. Figure 16 presents the graphite system.

The graphite system contains a 1 MeV, isotropic and uniformly distributed neutron source that extends axially from 84 cm to 99 cm. It is centred 143 cm from the centre line of the graphite cylinder and has a radius of 25 cm. The centreline of the source is in one of the defuelling chutes (see Figure 16). The fuel in the defuelling chute is modelled as a homogenised fuel region. A downward neutron current tally, which is a ring detector, is defined at the lower surface of the system. The radius of the ring is 144 cm and the centre of the ring is positioned at the lower surface of the system.

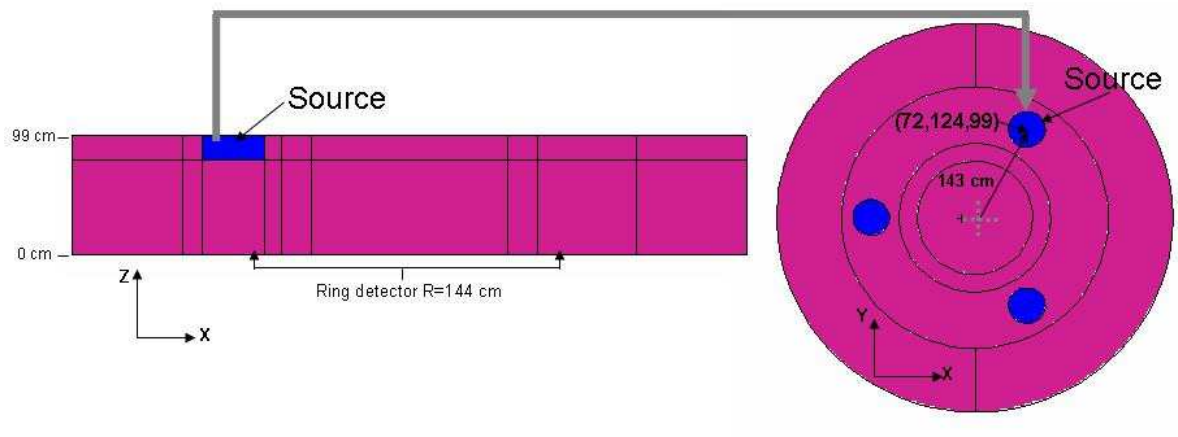

Figure 16: Vertical and Horizontal Section of the Graphite System

5.1.1 Weight Window Generation for the Graphite System

This section discusses the generation of one-group energy weight windows for the graphite cylinder. To determine weight windows for the system, some "synthetic" weight windows are used as a first approach to the problem of transporting particles from the source to the tally. With this approach good sampling of collisions, used to estimate the value of the final weight windows, are achieved if a ring detector is used. The synthetic weight windows are defined so that the importances have an exponential distribution throughout the system. A superimposed one-dimensional weight window mesh is used initially. These weight windows are shown in Figure 17.

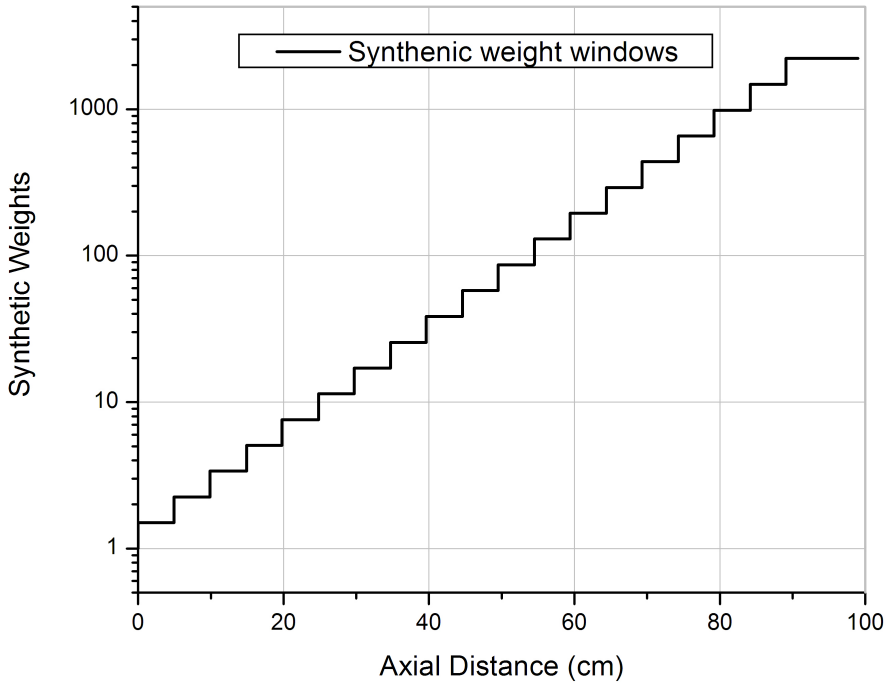

Figure 17: Initial Weight Windows

Subsequently, three different set-ups are considered. The geometry and the position of the tally for all the set-ups are kept the same as the original problem; only the definition of the source is changed. The neutron source for the first set-up is defined to be a 1 MeV uniformly distributed volumetric source extending axially from 59 cm to 99 cm with a 275 cm radius. Therefore, it covers the system in only this specific area. Considering the second set-up, the neutron source is defined as a 1 MeV uniformly distributed volumetric source extending axially from 29 cm to 69 cm with a 275 cm radius. For the third set-up the neutron source is defined as a 1 MeV uniformly distributed volumetric source extending axially from 0 cm to 40 cm and with a 275 cm radius. The source is divided into three sections because better source biasing can be achieved if the source is made smaller.

Next, the automatic weight window generator of MCNP is used to generate weight windows for each set-up by reading the synthetic weight windows. The new weight windows are generated in a three-dimensional rectangular mesh that suits the system better than the one-dimensional mesh used for the initial step of the synthetic weight windows. This leads to three sets of weight windows calculated for

the complete system, each one for a fixed source in a different part of the system. The next step is to unify the three sets into one. The reason for unifying the weight windows is to get a single set of weight windows that consists of good importance estimates for the whole domain. The positions of the sources and the unified weight windows are presented in Figure 18.

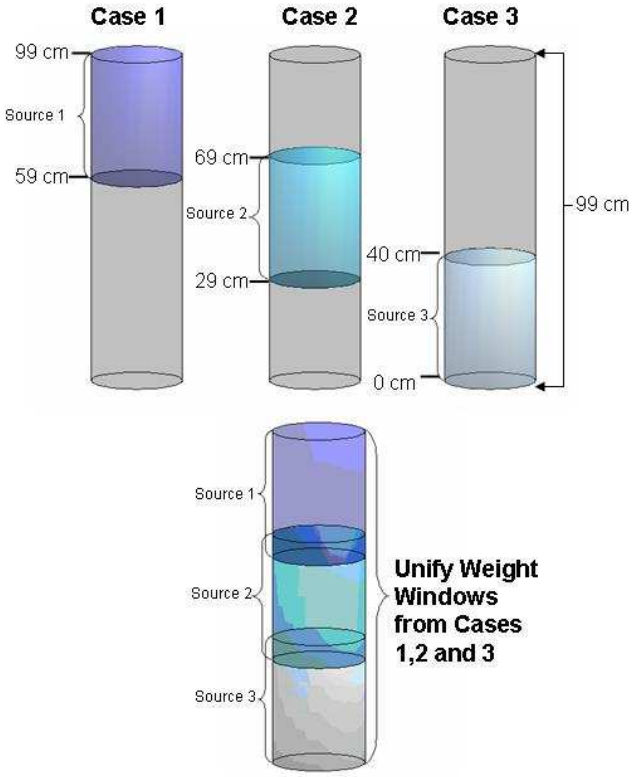

Figure 18: Unifying of Weight Windows for the Graphite System

5.1.2 Biasing the Neutron Source

A tool that has been developed at PBMR is used to do the source biasing (see Dorval (2008)). The tool has the capability of performing multi-group and one-group importance-based source biasing. To do source biasing, a biased source probability density function $\hat{q}$ is defined according to Equation (3.3.3). The tool makes use of this formulation to bias the weights of the source particles to have the same behaviour as the weight windows within the source region. Using a scaling factor makes it possible for the biased weights of the source particles to be within the one-group energy weight window bounds.

5.1.3 Results for the Graphite System

This section gives the results for different scenarios such as not using weight windows and for using weight windows and source-biasing consistent weight windows.

The results for the tally mean, relative error and FOM when the fissions are turned off are given for 1E+06 histories. The scenarios without weight windows have not passed all the convergence tests. On the other hand the scenario with weight windows and source-biasing consistent with weight windows have passed all the convergence test.

Compared to using no weight windows it is evident from Table 8 that by applying weight windows and source biasing consistent with weight windows the FOM is improved and the relative error is reduced.

Table 8: Results for the Graphite System using a Ring Detector (Fissions turned off)

Scenario	Tally Mean ($neutrons/cm^2-\sec$)	Relative error	FOM	Percentage particles outside window
No Weight Windows	1.50E-07	0.11	4.2	n/a
Source biasing consistent with Weight Windows	1.57E-07	0.008	105	21%

Next, take the fissions produced at the defuelling chutes into account. It is evident that the flux is approximately 20% higher than the first case. Results for the tally mean, relative error and FOM for only two scenarios are given in Table 9 for 1E+06 histories. The first scenario is without weight windows and the second scenario is with weight windows and source biasing consistent with weight windows. Comparing the two scenarios it is evident that the second scenario has a much higher FOM, which makes this scenario much more efficient.

Table 9: Results for the Graphite System using a Ring Detector (Fissions turned on)

Scenario	Tally Mean ($neutrons/cm^2 - \sec$)	Relative error	FOM	Percentage particles outside window
No Weight Windows	7.6E-07	0.03	4.6	n/a
Source biasing consistent with Weight Windows	7.43E-07	0.005	53	21%

Note that convergence is achieved faster when fissions in the defuel chutes are considered. This is because neutrons are produced closer to the tally compared with the case where there is only a neutron source at the top of the system.

5.1.4 Summary

The case presented in this chapter is based on a system similar to one axial reflector of the PBMR and illustrates an application of the concepts and methodologies described in the preceding chapters.

A method using predefined weight windows to generate weight windows was considered. Source biasing consistent with weight windows was applied in the process of generating weight windows. The source biasing was improved by dividing the neutron source into three sections. The three sets of weight windows were then unified to obtain good importance estimates for the whole system.

A tool developed within PBMR was used to bias the volumetric source and is based on the theory in Chapter 3.

In shielding calculations of the bottom reflector of the PBMR, fissions in the fuel inside the defuel chutes can contribute significantly to the neutron flux far from the reactor core, as shown in the example solved in this Chapter. In both cases, it was observed that the use of weight windows and source biasing consistent with weight windows improved the efficiency of the calculations. It was also observed that, as expected, considering fissions in the calculations takes more execution time than when they are not taken into account.

6. Conclusions

Chapter 1 and Chapter 2 gave an overview of the different variance reduction methods such as geometry splitting and weight windows. A summary of the advantages and disadvantages of these methods were presented in light of the cases analysed in this dissertation.

Three case studies were defined to investigate different methodologies on how to generate weight windows. The first study showed how to use the iterative method of moving ring detectors and the truncation method to generate weight windows. This is a very tedious procedure. The second study showed how to use geometry splitting to generate weight windows. One of the disadvantages is that this method requires that the geometry be split into different sections. Due to the small dimensions of the system the weight windows were generated in only one MCNP run. The third method made use of synthetic weight windows to generate weight windows for the whole system. Compared to the first method less time was taken to generate weight windows for this system. It was shown that all three methods produced good importance estimates for the different systems. Judgement should be used to determine which approach is more suitable. Some general pointers that should be taken into account when generating weight windows, to ensure the weight windows are well converged, are:

- If using point detectors in an iterative process, it is advisable to verify at each step the ratio of weight windows between adjacent cells. If a ratio is very high, the ring detector should be moved in smaller steps.
- The mesh sizes should be checked before the next generation of weight windows to make sure that there are no high weight ratios between adjacent cells. If high weight ratios occur between adjacent cells, the mesh sizes should be reduced. It should be taken into account that too-fine meshes can result in unnecessary calculations being performed that do not contribute to the quality of the calculation.
- When generating weight windows it is important to generate good weight windows at every iteration because bad weight windows cannot be overcome.

The best weight window used is where the Monte Carlo particles are distributed uniformly throughout the system. This will ensure firstly that all the sub-regions of the system are adequately sampled and secondly control the particle weights even in regions far from the source. A weight window can be referred to as good, if the tally used to generate weight windows has passed all the convergence tests. There should also be no high weight ratios between adjacent cells and important regions should not be filled with zero weight windows.

The biased source probability density function is given in Chapter 3. It was shown how to determine this biased source probability density function with weight windows generated with MCNP. By using the biased source probability density function the weights of the source particles are biased to be within the weight window bounds. It was shown that by doing this the efficiency of an MCNP calculation can be improved drastically.

Further, another two scenarios on source biasing were investigated. The first scenario biased the source so that the particles born in the region contributing more to the tally have weight within the weight window bounds and the rest have weight below the weight window bounds. The second scenario biased the source so that the particles born in the more important part of the source have weight within the weight window bounds. The rest of the source particles have weight above the weight window bounds. It was found that the first scenario is more efficient.

Weight windows generated for coupled neutron-photon problems can be used directly for photon-only problems if the photon source is well distributed throughout the system. To illustrate this concept two scenarios were considered i.e. an iron and a heavy concrete cylinder. Both these scenarios consist of high photon production cross-sections through neutron reactions. Two different approaches were followed to determine weight windows for each system. Considering the iron scenario, the methodology used was to run the automatic weight windows generator of MCNP in the system with a proper importance distribution for splitting and Russian roulette. The heavy concrete scenario used the iterative method of moving ring detectors and truncating the system to generate weight windows.

The analysis conducted in Chapter 5 is an introduction to show how the particle transport problem of the bottom reflector of the PBMR can be solved. It was shown that weight windows and source biasing consistent with weight windows improves the efficiency of the calculations. It has been noted that when performing shielding calculations, for systems like the bottom reflector of the PBMR, fissions in the fuel inside the defuel chutes can have a significant contribution to the neutron flux far from the reactor core, as shown in the example solved in Chapter 5.

7. BIBLIOGRAPHY

Booth, T.E. 1985. A Sample Problem for Variance Reduction in MCNP. (Report No. LA-10363-MS). Los Alamos: Los Alamos National Laboratory.

Booth, T.E., Brown, F.B, Bull, J.S, Foster, R.A.,Goorley, J.T, Hughes, H.G, Mosteller R.D, Prael, R.E, Sood, A., Sweezy, J.E., Zukaitis, A., Boggs, M., Martz, R. 2003. MCNP-A General Monte Carlo N-Particle Transport Code, Version 5. (Report No. LA-CP-03-0245). Los Alamos: Los Alamos National Laboratory.

Brown, F.P.2000. Fundamentals of Monte-Carlo Particle Transport. (Report No. LA-UR-05-4983). . Los Alamos: Los Alamos National Laboratory.

Culbertson, C.N. and Hendricks, J.S. 1999. An Assessment of the MCNP4C Weight Window. (Report No. LA-13668). Los Alamos: Los Alamos National Laboratory.

Conveyou, R.R, Cain, V.R and Yost, K.J. 1967. Adjoint and Importance in Monte Carlo application. Nucl. Sci. Eng.,27,219.

Dorval, E. 2008 Weight Window Based Source Biasing for MCNP Calculations. (Report No. DIT001126). Centurion: Pebble Bed Modular Reactor (Pty) Ltd.

Koster, A. 2008. Technical Description of the PBMR Demonstration Power Plant. (Report No. 016956/5). Centurion: Pebble Bed Modular Reactor (Pty) Ltd.

Lewis, E.E. and Miller, W.F.1984. Computational Methods of Neutron Transport. 1st ed. John Wiley and Sons Inc.

Lamarsh, J.R. and Baratta, A.J. 2001. Introduction to Nuclear Engineering. 3rd ed. Prentice-Hall Inc.

Prinsloo, P. 2006. Core Structures Ceramics Design Description. (Report No. 026224/D). Centurion: Pebble Bed Modular Reactor (Pty) Ltd.

Radulescu, G. 2003. Automated Variance Reduction for Monte Carlo Shielding Analyses with MCNP. Ph. D. The University of Texas at Austin.
Tiro, K. 2009. Reactor Model Flow Model Report. (Report No. T000330/4). Centurion: PBMR (Pty) Limited Centurion.

Ozgener, A. 2006. On the Monte Carlo Method. North West University. [Course notes for Advanced II Reactor Analysis –MSc Nuclear Engineering NWU]

Wagner, J.C. and Haghighat, A. 2003. Monte Carlo Variance Reduction with Deterministic Important Functions. Progress in Nuclear Energy, Vol.42, No.1, pp.25-53.